PNAS
www.pnas.org

Supplementary Information for

Effects of Knot Tightness at the Molecular Level

Liang Zhang[a,b], Jean-François Lemonnier[b], Angela Acocella[c], Matteo Calvaresi[c], Francesco Zerbetto*[c] and David A. Leigh[a,b]*

a. School of Chemistry and Molecular Engineering, East China Normal University, 200062 Shanghai, China
b. School of Chemistry, University of Manchester, Oxford Road, Manchester, M13 9PL, United Kingdom
c. Dipartimento di Chimica "G. Ciamician", Universita' di Bologna, V. F. Selmi 2, 40126, Bologna, Italy

Francesco Zerbetto and David A. Leigh
Email: david.leigh@manchester.ac.uk; franceso.zerbetto@unibo.it

This PDF file includes:

Synthetic procedures and characterisation details of organic knots **1**-**3** and corresponding intermediates. NMR and MS spectra of organic knots **1**-**3** and corresponding intermediates. UV, tandem mass spectra, chiral HPLC resolution and computational information of organic knots.
Scheme S1 to S5
Figs. S1 to S38
Tables S1
References for SI reference citations

S1. General Experimental Section Unless stated otherwise, all reagents and solvents were purchased from Sigma-Aldrich Chemicals and used without further purification. Dry solvents were obtained by passing through an activated alumina column on a Phoenix SDS solvent drying system (JC Meyer Solvent Systems, CA, USA). NMR spectra were recorded on a BrukerAvance III (equipped with a cryoprobe) instrument with an Oxford AS600 magnet. Chemical shifts are reported in parts per million (ppm) from high to low frequency and referenced to the residual solvent resonance. N^{th} order coupling constants (^{n}J) are reported in Hertz (Hz). Standard abbreviations indicating multiplicity were used as follows: s = singlet, d = doublet, t = triplet, q = quartet, quin = quintet, m = multiplet, br = broad. ^{1}H assignments were made using 2D NMR methods (COSY, HSQC, HMBC). Variable temperature and DOSY NMR spectra were recorded on a Bruker Avance II+ instrument (500 MHz). Low resolution ESI mass spectrometry was performed with a Thermo Scientific LCQ Fleet or an Agilent Technologies 1200 LC system with 6130 single quadrupole MS detector mass spectrometer. High resolution ESI (electrospray ionization) and EI (electron ionization) mass spectrometry were carried out by the mass spectrometry services at the University of Manchester or by the mass spectrometry services at the EPSRC National MassSpectrometry Service Centre, Swansea, UK. MALDI-TOF measurements were performed with a Shimadzu Axima Confidence using DCTB as matrix and NaI as an additive. All circular dichroism (CD) spectra were recorded on a J-815 Jasco spectrometer (Jasco France, Nantes, France). Spectra were acquired between 215 and 400 nm in dichloromethane (spectrophotometric grade) using a quartz cell with a path length of 1 mm. Sample temperature was regulated at 20°C with the solvent and concentration stated. Optical rotation measurements were taken on an API/1W automatic polarimeter with the solvent and concentration stated in a 25 mm cuvette. High Performance Liquid Chromatography (HPLC) purifications and analysis were carried out in an Agilent 1200 series HPLC using a 4.6 mm x 250 mm Chiralpak® IF column (particle size 5 μm, flow rate 1.0 ml/min, 254 nm detector). Compounds **S3**, **S4**, **L1**, **$[Fe_4L1_4](PF_6)_8$**, **$[Fe_41](PF_6)_8$** and **1** were synthesized according to literature procedures.[1]

S2. Synthetic Overview

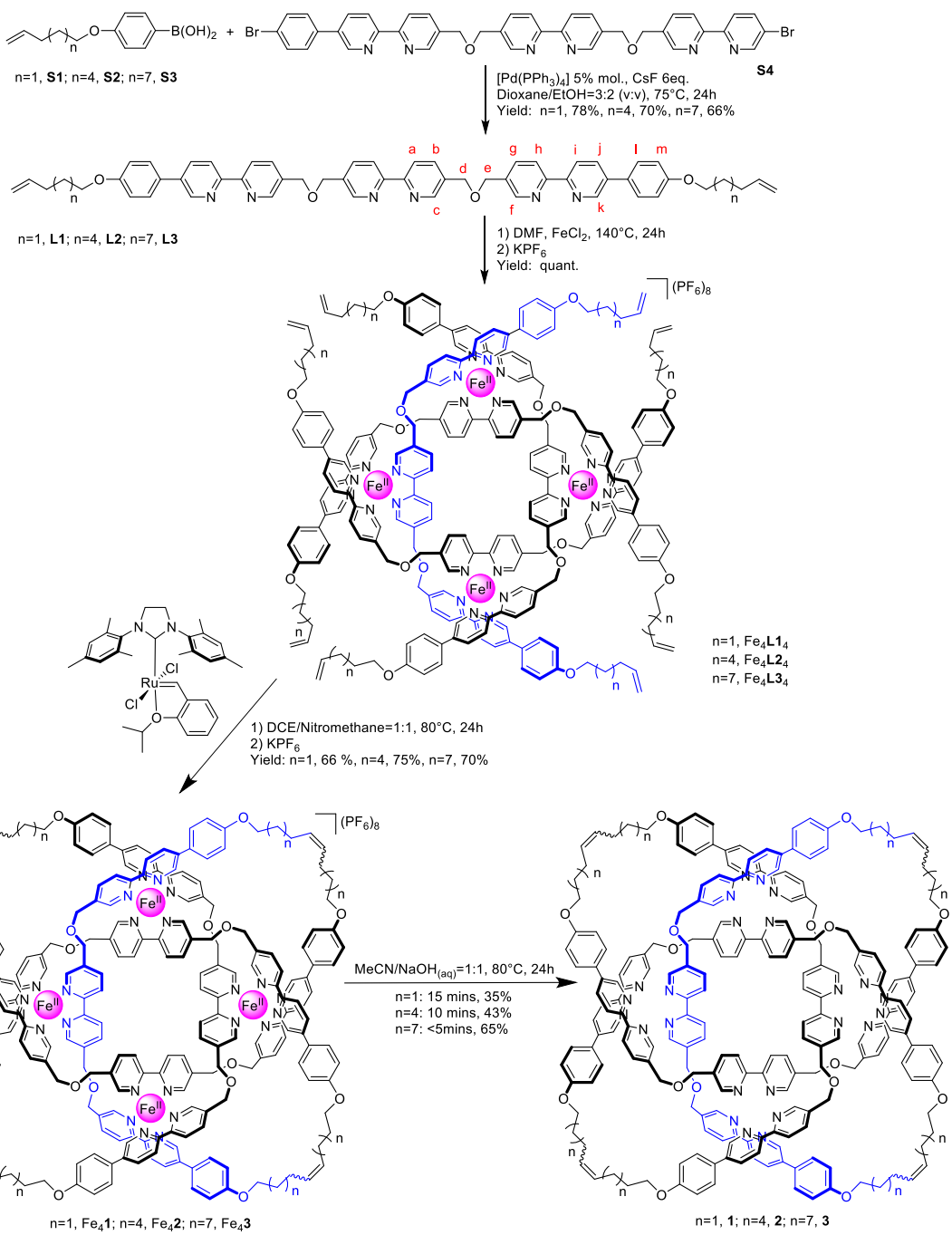

Scheme S1. Synthesis of molecular knots **1-3**.

S3. Synthetic procedures and characterization details

S3.1 General Procedure for the Synthesis of Boronic Acid **S1-S3**

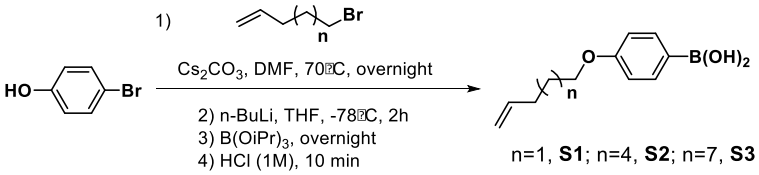

Scheme S2. Synthesis of Boronic Acid **S1-S3**

General Procedure: 4-Bromophenol (30 mmol, 1 equiv.) and Br-substituted-1-ene (45 mmol, 1.5 equiv.) were dissolved in DMF (100 mL). Cs_2CO_3 (9.8 g, 30 mmol, 1 equiv.) was added and the resulting suspension heated to 70°C for overnight. The mixture was filtered, and the solvent removed under reduced pressure. The brown oil was dissolved in DCM (100 mL) and washed by water (20 mL) and brine (20 mL), dry by $MgSO_4$ and the solvent removed and leave under high vacuum for overnight to get colourless oil. Take all the oil and dissolve in anhydrous THF (200 mL) and cooled to -78°C. *n*-Butyllithium (1.6 M in hexanes, 20 mL, 1 equiv.) was added and the resulting mixture stirred for 2 hours at -78°C. B(O*i*Pr)$_3$ (50 mL) was quickly added and the mixture was allowed to reach ambient temperature overnight. Aq. HCl (1 M, 100 mL) was added and the mixture stirred for 10 min. CH_2Cl_2 (500 mL) and brine (500 mL) were added, the organic layer isolated and the solvent removed under reduced pressure. The crude product was washed with petroleum ether to yield the corresponding boronic acid.

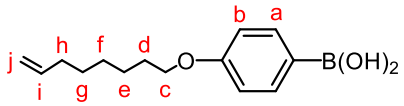

S2

Following the general procedure, **S2** was isolated as a colorless solid (6.3 g, 25.5 mmol) in 85% yield.

^{1}H NMR (600 MHz, $CDCl_3$) δ 8.15 (d, J = 9.0 Hz, 2H, H^a), 7.00 (d, J = 8.8 Hz, 2H, H^b), 5.87 – 5.77 (m, 1H, H^i), 5.04 – 4.91 (m, 2H, H^j), 4.05 (t, J = 6.4, 2H, H^c), 2.10 – 2.04 (m, 2H, H^d), 1.86 – 1.79 (m, 2H, H^e), 1.54 – 1.35 (m, 6H, H^f, H^g, H^h). ^{13}C NMR (151 MHz, $CDCl_3$) δ 162.89, 139.16, 137.61, 114.46, 114.12, 67.94, 66.02, 33.87, 29.33, 29.02, 28.97, 26.07, 15.43. HRESI-MS: calcd. for $C_{14}H_{21}BO_3$+H$^+$ 249.31657 found 249.1657.

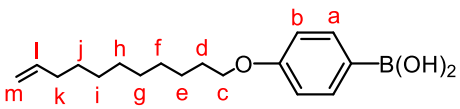

S3

Following the general procedure, **S3** was isolated as a colorless solid (7.1 g, 24.6 mmol) in 82% yield.

^{1}H NMR (600 MHz, $CDCl_3$) δ 8.15 (d, J = 8.0 Hz, 2H, H^a), 7.00 (d, J = 8.8 Hz, 2H, H^b), 5.87 – 5.77 (m, 1H, H^l), 5.03 – 4.90 (m, 2H, H^m), 4.07 (t, J = 6.4, 2H, H^c), 2.08 – 1.99 (m, 2H, H^d), 1.86 – 1.73 (m, 2H, H^e), 1.51 – 1.21 (m, 12H, H^{f-k}). ^{13}C NMR (151 MHz, $CDCl_3$) δ 162.78, 139.25, 137.47, 135.24, 129.40, 114.14, 114.13, 114.00, 67.88, 33.83, 29.53, 29.44, 29.41, 29.24, 29.14, 28.94, 26.06, 15.30. HRESI-MS: calcd. for $C_{17}H_{27}BrO_3$+H^+ 359.1216 found 359.1214.

S3.2 General Procedure for the Synthesis of Ligand **L1**- **L3**

General Procedure: **S4** (0.50 mmol, 1 equiv.), boronic acid **S1**, **S2** or **S3** (1.46 mmol, 2.9 equiv.) and caesium fluoride (500 mg, 3.3 mmol, 6.6 equiv.) were added to a dried schlenk vessel under a positive nitrogen atmosphere and then suspended in a mixture of dioxane (15 mL) and ethanol (10 mL). The resulting turbid pale yellow solution was degassed by nitrogen bubbling for 20 min under vigorous stirring and extra 20 min after addition of $Pd(PPh_3)_4$ (29 mg, 0.025 mmol, 5 mol%). The reaction was stirred and heated for 24 h at 75°C. The resulting pale brown solution was poured in CH_2Cl_2 (100 mL) and washed successively with aqueous sat. $NaHCO_3$ solution (150 mL), water (150 mL) and brine (150 mL). The combined aqueous phases were mixed and extracted with CH_2Cl_2 (100 mL). The combined organic phases were collected, dried over Na_2SO_4 and the solvent removed under reduced pressure to give a pale brown solid. The crude material was suspended in methanol (100 mL) and refluxed for 24 h. The pale brown solid was isolated by filtration and the process was repeated twice to finally afford the pure corresponding ligand.

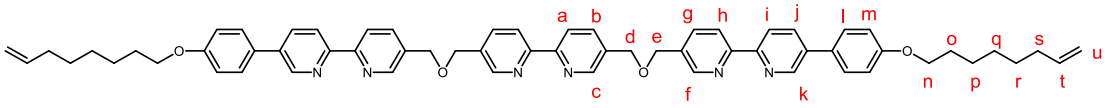

L2

Following the general procedure, **L2** was isolated as beige solid (335 mg, 0.35 mmol) in 70% yield.

^{1}H NMR (600 MHz, $CDCl_3$) δ 8.89 (d, J = 2.4 Hz, 2H, H^k), 8.70 – 8.66 (m, 4H, H^c, H^f), 8.46 – 8.40 (m, 6H, H^a, H^i, H^h), 7.98 (dd, J = 8.2, 2.4 Hz, 2H, H^j), 7.87 (d, J = 2.4 Hz, 2H, H^b), 7.85 (d, J = 2.4 Hz, 2H, H^g), 7.59 (d, J = 8.7 Hz, 4H, H^l), 7.02 (d, J = 8.7 Hz, 4H, H^m), 5.93 – 5.86 (m, 2H, H^t), 5.13 – 5.03 (m, 4H, H^u), 4.70 (s, 8H, H^d, H^e), 4.01 (t, J = 6.4 Hz, 4H, H^n), 2.11 – 2.03 (m, 4H, H^o), 1.85 – 1.77 (m, 4H, H^p), 1.53 – 1.35 (m, 12H, $H^{q,r,s}$). ^{13}C NMR (151 MHz, $CDCl_3$) δ 159.58, 155.91, 155.77, 154.13, 148.85, 148.83, 147.40, 139.16, 136.68, 136.37, 134.79, 133.50, 133.22, 129.87, 128.28, 121.13, 121.08, 120.90, 115.29, 114.47, 70.03, 69.97, 68.24, 33.87, 31.11, 29.34, 29.00, 28.98, 26.06. HRESI-MS: calcd. for $C_{62}H_{64}N_6O_4$+H^+ 957.5062 found 957.5060. m. p. 277 – 279°C.

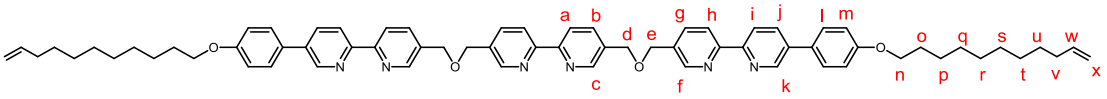

L3

Following the general procedure, **L3** was isolated as beige solid (344 mg, 0.33 mmol) in 66% yield.

^{1}H NMR (600 MHz, $CDCl_3$) δ 8.91 (d, J = 2.4 Hz, 2H, H^k), 8.73 – 8.69 (m, 4H, H^c, H^f), 8.48 – 8.43 (m, 6H, H^a, H^i, H^h), 8.00 (dd, J = 8.2, 2.4 Hz, 2H, H^j), 7.90 (d, J = 2.4 Hz, 2H, H^b), 7.88 (d, J = 2.4 Hz, 2H, H^g), 7.61 (d, J = 8.7 Hz, 4H, H^l), 7.05 (d, J = 8.7 Hz, 4H, H^m), 5.89 – 5.80 (m, 2H, H^t), 5.05 – 4.94 (m, 4H, H^u), 4.72 (s, 8H, H^d, H^e), 4.04 (t, J = 6.6 Hz, 4H, H^n), 2.10 – 2.04 (m, 4H, H^o), 1.87 – 1.80 (m, 4H, H^p), 1.53 – 1.46 (m, 4H, H^q), 1.44 – 1.27 (m, 20H, $H^{r\text{-}v}$). ^{13}C NMR (151 MHz, $CDCl_3$) δ 159.35, 155.64, 155.51, 153.85, 148.64, 147.09, 136.40, 135.92, 134.35, 133.41, 133.09, 130.44, 130.00, 129.63, 128.05, 120.92, 120.90, 120.72, 115.10, 69.93, 69.84, 68.08, 46.22, 32.83, 29.86, 29.64, 29.54, 29.48, 29.30, 27.46, 26.12. HRESI-MS: calcd. for $C_{68}H_{76}N_6O_4$+H^+ 1041.6001 found 1041.6000. m. p. 285 – 287°C.

S3.3 General Procedure for the Synthesis of Circular Helicate $[Fe_4\mathbf{L}_4](PF_6)_8$

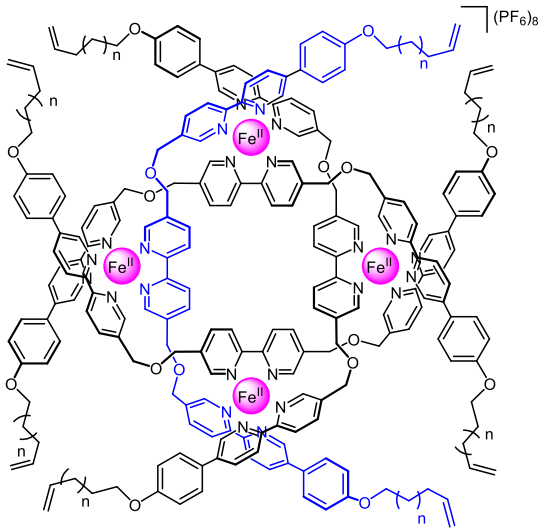

n=1, Fe_4**L1**$_4$; n=4, Fe_4**L2**$_4$; n=7, Fe_4**L3**$_4$

General Procedure: **Ligand** (50 µmol, 1 equiv.) was combined with $FeCl_2$ (50 µmol, 1 equiv.) and degassed DMF (5.7 mL) under an atmosphere of nitrogen. The reaction mixture was stirred and heated to 130°C in a sealed vial for 24 h, then cooled to room temperature. A saturated solution of KPF_6 in methanol was added to the purple solution until a precipitate formed, which was subsequently collected by filtration onto celite and washed with excess water. The remaining solid was dissolved in acetonitrile, and the solvent removed under reduced pressure to yield corresponding circular helicate.

Following the general procedure, [Fe_4**L2**$_4$](PF_6)$_8$ was isolated as purple solid (261 mg, 50 µmol) in quantitative yield. The lettering corresponds to the proton labelling in ligand **L2**.

^{1}H NMR (600 MHz, CD_3CN) δ 9.36 (d, J = 5.0 Hz, 8H, H^a), 8.50 (d, J = 8.4 Hz, 8H, H^h), 8.48 (d, J = 8.4 Hz, 8H, H^i), 8.26 (dd, J = 8.6, 1.4 Hz, 8H, H^j), 7.96 (d, J = 8.5 Hz, 8H, H^g), 7.77 (d, J = 8.2 Hz, 8H, H^b), 7.58 (s, 8H, H^f), 7.36 (s, 8H, H^c), 7.31 (s, 8H, H^k), 7.24 (d, J = 8.5 Hz, 16H, H^l), 6.91 (d, J = 8.7 Hz, 16H, H^m), 5.87 – 5.75 (m, 8H, H^t), 4.99 (dd, J = 17.2, 1.4 Hz, 8H, H^u-cis), 4.92 (d, J = 10.2 Hz, 8H, H^u-trans), 4.75 – 4.65 (m, 16H, H^e), 4.43 – 4.33 (m, 16H, H^d), 3.96 (t, J = 6.5 Hz, 16H, H^n), 2.04 (q, J = 7.0 Hz, 16H, H^s), 1.73 (quin, J = 7.2 Hz, 16H, H^o), 1.50 – 1.23 (m, 48H, H$^{p\text{-}r}$). ^{13}C NMR (151 MHz, CD_3CN) δ 161.43, 159.57, 157.65, 153.05, 151.36, 151.21, 140.32, 140.07, 139.47, 139.03, 138.58, 136.87, 136.69, 129.20, 127.51, 124.92, 124.09, 116.27, 114.86, 69.91, 69.50, 69.03, 36.55, 34.35, 31.26, 29.73, 29.70, 29.56, 29.49, 26.46. LRESI-MS: *m/z* = 1592.17 [M–3PF_6]$^{3+}$ requires 1592.68; 1157.67 [M–4PF_6]$^{4+}$ requires 1157.90; 897.33 [M–5PF_6]$^{5+}$ requires 897.62; 723.67 [M– 6PF_6]$^{6+}$ requires 723.86. HRESI-MS: *m/z* = 1157.8889 [M–4PF_6]$^{4+}$ (calcd. for $C_{248}H_{256}N_{24}O_{16}Fe_4P_4F_{24}$, 1157.8991).

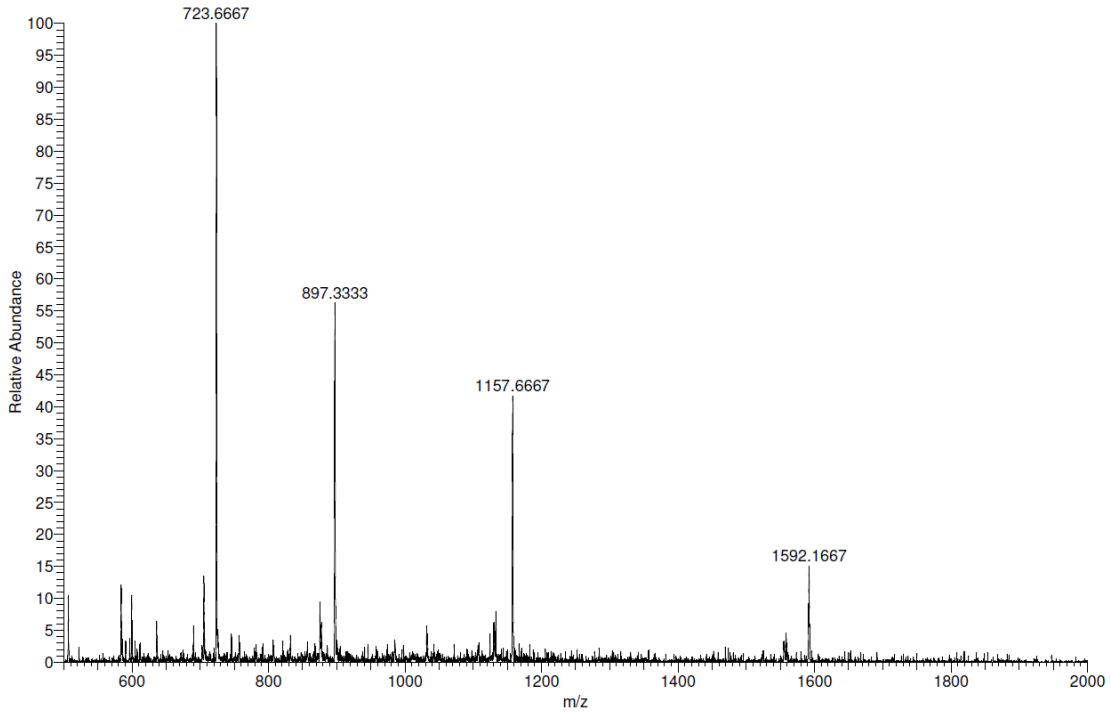

Fig. S1. Low-resolution ESI-MS of circular helicate $[Fe_4\mathbf{L2}_4](PF_6)_8$. Calculated peaks (*m/z*) 1592.68 $[M\text{-}3PF_6]^{3+}$, 1158.27 $[M\text{-}4PF_6]^{4+}$, 897.62 $[M\text{-}5PF_6]^{5+}$, 723.86 $[M\text{-}6PF_6]^{6+}$.

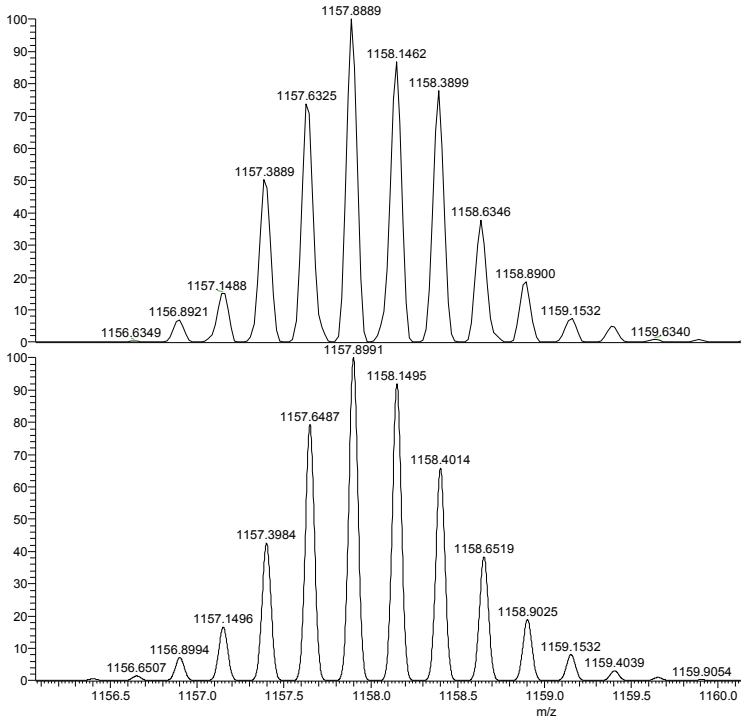

Fig. S2. HRESI-MS of $[M–4(PF_6)]^{4+}$ peak of $[Fe_4\mathbf{L2}_4](PF_6)_8$. Experimental spectrum (top) and calculated spectrum (bottom).

Following the general procedure, $[Fe_4\mathbf{L3}_4](PF_6)_8$ was isolated as purple solid (277 mg, 50 μmol) in quantitative yield. The lettering corresponds to the proton labelling in ligand **L3**.

^{1}H NMR (600 MHz, CD_3CN) δ 9.36 (br, 8H, H^a), 8.49 (d, J = 8.6 Hz, 8H, H^h), 8.47 (d, J = 8.6 Hz, 8H, H^i), 8.26 (dd, J = 8.5, 1.3 Hz, 8H, H^j), 7.96 (d, J = 8.4 Hz, 8H, H^g), 7.78 (d, J = 6.5 Hz, 8H, H^b), 7.59 (s, 8H, H^f), 7.35 (s, 8H, H^c), 7.29 (s, 8H, H^k), 7.23 (d, J = 8.6 Hz, 16H, H^l), 6.91 (d, J = 8.7 Hz, 16H, H^m), 5.87 – 5.75 (m, 8H, H^w), 4.99 (dd, J = 17.2, 1.4 Hz, 8H, H^x-cis), 4.92 (d, J = 10.2 Hz, 8H, H^x-trans), 4.76 – 4.64 (m, 16H, H^e), 4.43 – 4.30 (m, 16H, H^d), 3.96 (t, J = 6.5 Hz, 16H, H^n), 2.03 (q, J = 7.1 Hz, 16H, H^v), 1.73 (quin, J = 7.6 Hz, 16H, H^o), 1.47 – 1.18 (m, 94H, $H^{p\text{-}u}$). ^{13}C NMR (151 MHz, CD_3CN) δ 161.45, 159.52, 157.63, 152.99, 151.16, 140.32, 140.19, 139.36, 139.02, 138.63, 136.67, 129.18, 127.47, 124.93, 124.06, 116.26, 114.76, 114.73, 69.90, 69.53, 69.06, 34.46, 30.20, 30.09, 30.00, 29.82, 29.80, 29.67, 26.62. LRESI-MS: *m/z* = 1704.25 $[M–3PF_6]^{3+}$ requires 1704.55; 1241.03 $[M–4PF_6]^{4+}$ requires 1242.18; 964.58 $[M–5PF_6]^{5+}$ requires 964.75; 779.75 $[M– 6PF_6]^{6+}$ requires 779.67, 647.67 $[M– 7PF_6]^{7+}$ requires 647.69. HRESI-MS: *m/z* = 779.6738 $[M–6PF_6]^{6+}$ (calcd. for $C_{272}H_{304}N_{24}O_{16}Fe_4P_2F_{12}$, 779.6740).

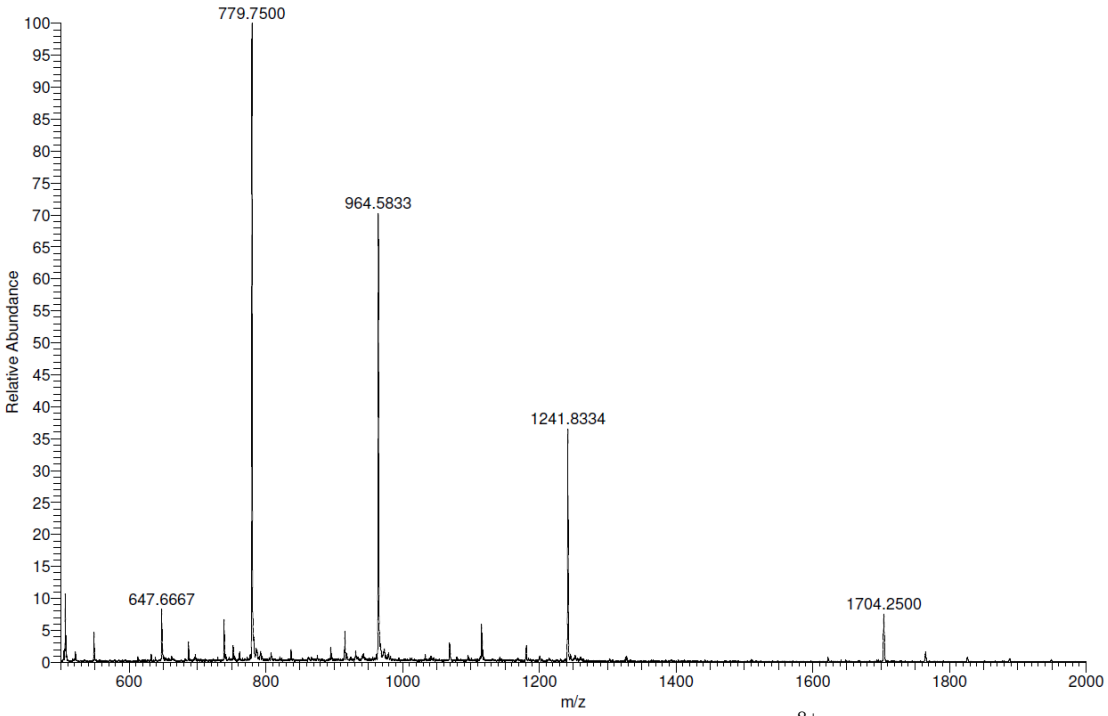

Fig. S3. Low-resolution ESI-MS of metallic knot $[Fe_4\mathbf{L3}]^{8+}$. Calculated peaks (*m/z*) 1704.55 $[M\text{-}3PF_6]^{3+}$, 1242.18 $[M\text{-}4PF_6]^{4+}$, 964.75 $[M\text{-}5PF_6]^{5+}$, 779.79 $[M\text{-}6PF_6]^{6+}$, 647.69 $[M\text{-}6PF_7]^{7+}$.

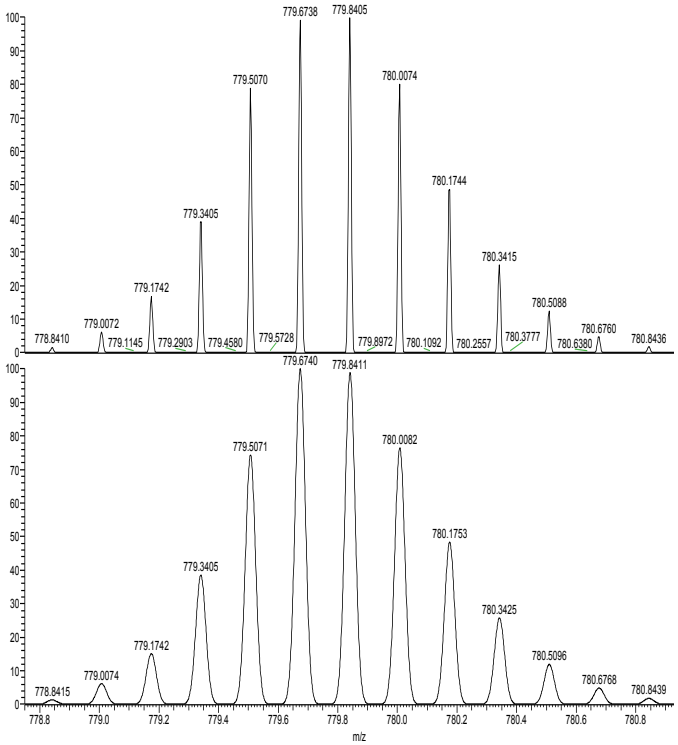

Fig. S4. HRESI-MS of $[M–6(PF_6)]^{6+}$ peak of $[Fe_4\mathbf{L3}_4](PF_6)_8$. Experimental spectrum (top) and calculated spectrum (bottom).

S3.4 General Procedure for the Synthesis of Metallic Knots $[Fe_4\mathbf{K}](PF_6)_8$

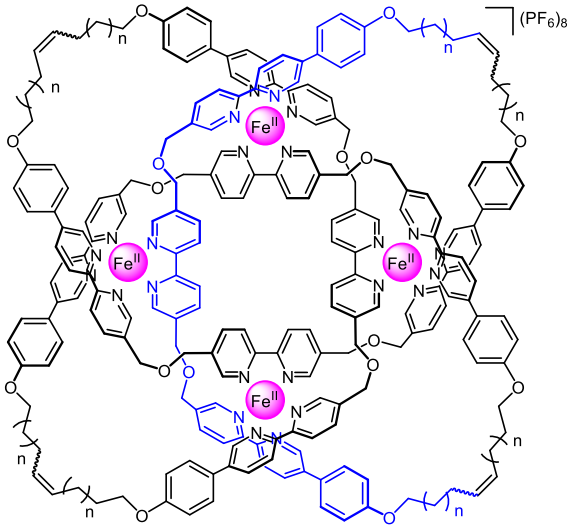

n=1, Fe_4**1**; n=4, Fe_4**2**; n=7, Fe_4**3**

General Procedure: Circular Helicate (10 μmol, 1 equiv.) dissolved in anhydrous and degassed nitromethane (5.2 mL) was added to an oven dried flask fitted with a magnetic stirrer bar under argon. Hoveyda-Grubbs second generation catalyst (6.3 mg, 10 μmol, 1 equiv.) was added as a solution in 1,2-dichloroethane (5.2 mL), and the reaction heated to 60°C for 24 h. Once cooled to room temperature, ethylvinyl ether was added, and the solution stirred for a further 30 minutes before removing the solvent under reduced pressure. The residue was sonicated in chloroform (25 mL) for 15 min, filtered onto celite, and washed with an excess of fresh chloroform. The remaining solid was dissolved in acetonitrile, and a saturated aqueous solution of KPF_6 was added until a precipitate formed. The precipitate was isolated by filtration onto celite, washed with excess water, and dissolved in acetonitrile. Removal of solvent under reduced pressure afforded the corresponding product.

Following the general procedure, $[Fe_4\mathbf{2}](PF_6)_8$ was isolated as purple solid (38.2 mg, 0.75 μmol) in 75% yield. The lettering corresponds to the proton labelling in ligand **L2**.

^{1}H NMR (600 MHz, CD_3CN) δ 9.38 (br, 8H, H^a), 8.49 (d, J = 8.8 Hz, 8H, H^h), 8.87 (d, J = 8.6 Hz, 8H, H^i), 8.27 (d, J = 8.2 Hz, 8H, H^j), 7.96 (d, J = 8.3 Hz, 8H, H^g), 7.79 (d, J = 6.1 Hz, 8H, H^b), 7.56 (s, 8H, H^f), 7.43 – 7.19 (m, 32H, $H^{c,k,l}$), 6.92 (d, J = 8.5 Hz, 16H, H^m), 5.44 – 5.32 (m, 8H, H^t), 4.78 – 4.63 (m, 16H, H^e), 4.44 – 4.30 (m, 16H, H^d), 4.02 – 3.86 (m, 16H, H^n), 2.10 – 2.01 (m, 16H, H^s), 1.77 – 1.65 (m, 16H, H^o), 1.49 – 1.23 (m, 48H, $H^{p\text{-}r}$). ^{13}C NMR (151 MHz, CD_3CN) δ 161.48, 159.62, 158.66, 157.67, 153.15, 151.02, 140.33, 139.45, 139.02, 138.66, 136.92, 136.74, 131.49, 130.84, 129.19, 127.41, 125.43, 124.91, 124.09, 116.20, 69.94, 69.54, 69.09, 32.63, 30.08, 29.83, 29.79, 29.61, 29.25, 28.70, 27.36, 26.20. LRESI-MS: *m/z* = 1518.17 $[M–3PF_6]^{3+}$ requires 1518.77; 1102.08 $[M–4PF_6]^{4+}$ requires 1102.84; 853.08 $[M–5PF_6]^{5+}$ requires 853.28; 686.92 [M–

$6PF_6]^{6+}$ requires 686.91, 568.08 $[M– 7PF_6]^{7+}$ requires 568.06. HRESI-MS: m/z = 686.7552 $[M–6PF_6]^{6+}$ (calcd. for $C_{240}H_{240}N_{24}O_{16}ClFe_4PF_6$, 686.7585).

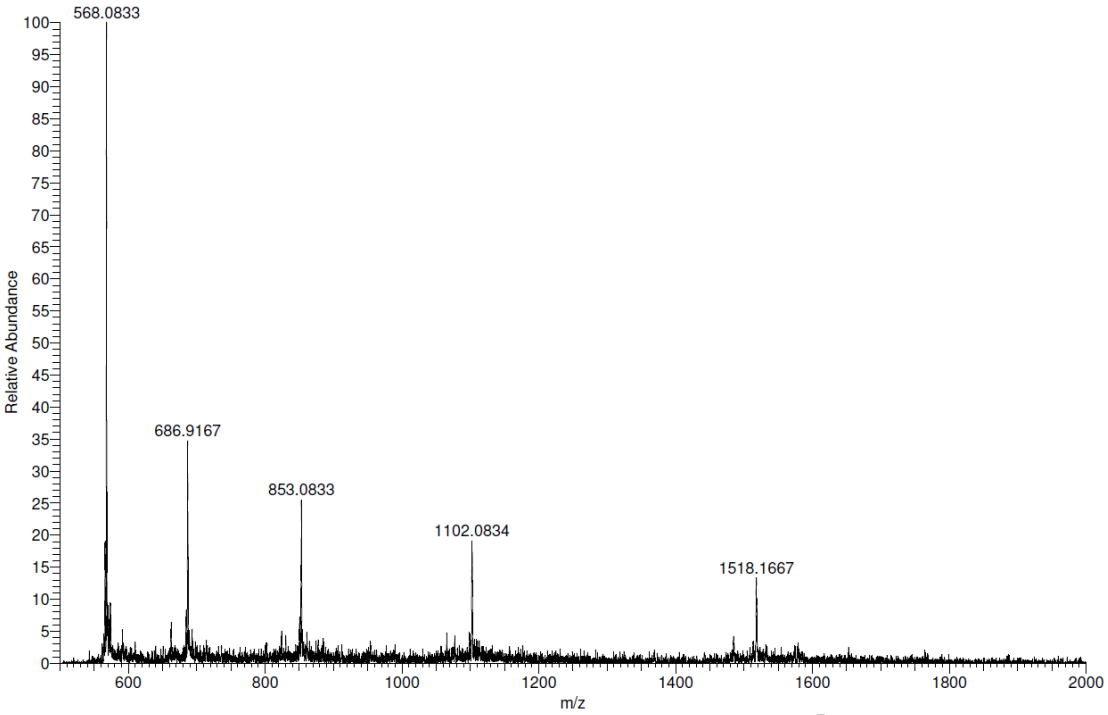

Fig. S5. Low-resolution ESI-MS of circular helicate $[Fe_4\mathbf{2}•Cl]^{7+}$. Calculated peaks (*m/z*) 1518.77 $[M–3PF_6]^{3+}$, 1102.84 $[M–4PF_6]^{4+}$, 853.28 $[M-5PF_6]^{5+}$, 686.91 $[M-6PF_6]^{6+}$, 568.06 $[M-7PF_6]^{7+}$.

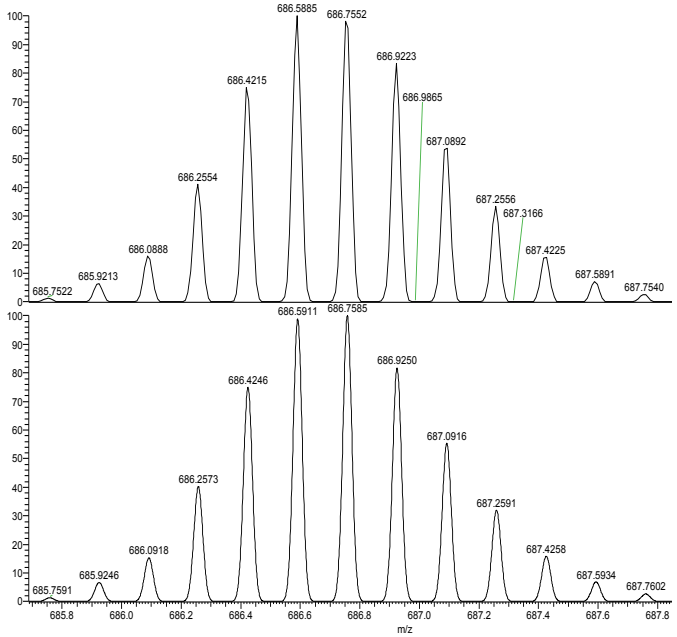

Fig. S6. HRESI-MS of $[M–6(PF_6)]^{2+}$ peak of $[Fe_4\mathbf{2}](Cl)(PF_6)_7$. Experimental spectrum (top) and calculated spectrum (bottom).

Following the general procedure, $[Fe_4\mathbf{3}](PF_6)_8$ was isolated as purple solid (38.1 mg, 0.75 μmol) in 70% yield. The lettering corresponds to the proton labelling in ligand **L3**.

^{1}H NMR (600 MHz, CD_3CN) δ 9.36 (br, 8H, H^a), 8.48 (br, 16H, $H^{h,i}$), 8.26 (br, 8H, H^j), 7.96 (br, 8H, H^g), 7.77 (br, 8H, H^b), 7.57 (s, 8H, H^f), 7.44 – 7.12 (m, 32H, $H^{c,k,l}$), 6.91 (br, 16H, H^m), 5.36 (s, 8H, H^w), 4.82 – 4.57 (m, 16H, H^e), 4.47 – 4.24 (m, 16H, H^d), 4.02 – 3.84 (m, 16H, H^n), 2.08 – 1.93 (m, 16H, H^s), 1.78 – 1.65 (m, 16H, H^o), 1.51 – 1.08 (m, 96H, H^{p-u}). ^{13}C NMR (151 MHz, CD_3CN) δ 161.47, 159.57, 158.66, 157.67, 153.04, 151.32, 151.15, 140.36, 139.42, 139.04, 138.62, 136.87, 136.72, 131.59, 130.92, 129.22, 127.50, 125.53, 124.92, 124.09, 116.20, 69.90, 69.53, 69.19, 32.73, 30.88, 30.14, 30.05, 30.01, 29.92, 29.89, 29.83, 29.59, 29.45, 28.83, 27.42, 26.72, 26.68, 22.40. LRESI-MS: *m/z* = 1630.00 $[M–3PF_6]^{3+}$ requires 1630.60; 1186.33 $[M–4PF_6]^{4+}$ requires 1186.71; 920.17 $[M–5PF_6]^{5+}$ requires 920.38; 742.83 $[M– 6PF_6]^{6+}$ requires 742.82; 616.00 $[M–7PF_6]^{7+}$ requires 616.00. HRESI-MS: m/z = 742.8181 $[M–6PF_6]^{6+}$ (calcd. for $C_{264}H_{288}N_{24}O_{16}Fe_4ClPF_6$, 742.8208).

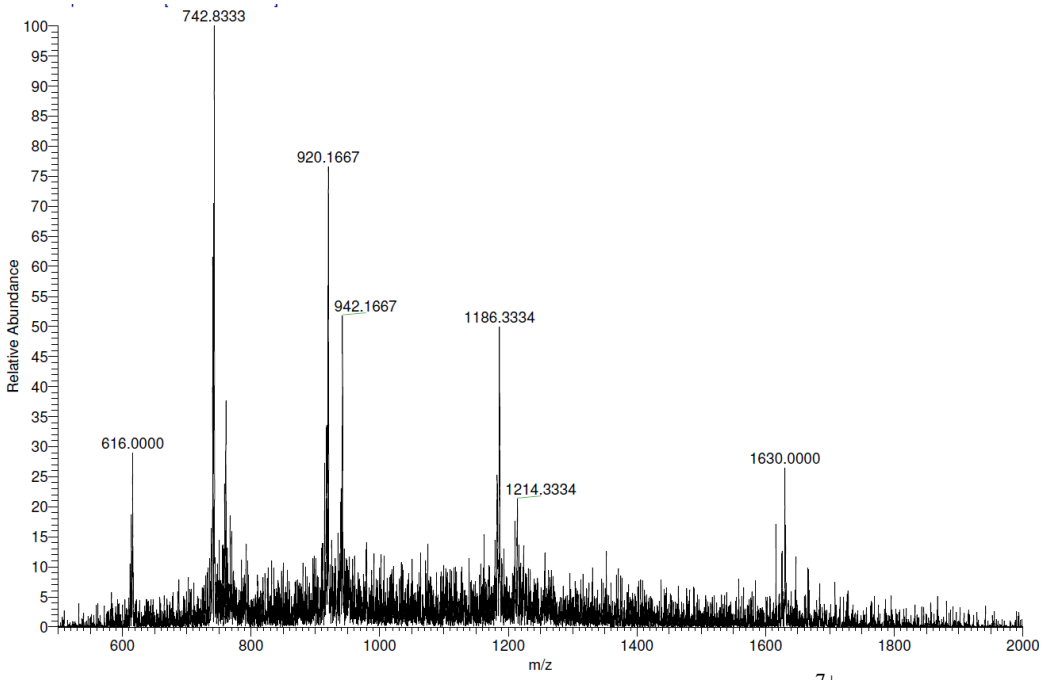

Fig. S7. Low-resolution ESI-MS of circular helicate $[Fe_4\mathbf{3}•Cl]^{7+}$. Calculated peaks (*m/z*) 1630.60 $[M\text{-}3PF_6]^{3+}$, 1186.71 $[M\text{-}4PF_6]^{4+}$, 920.38 $[M\text{-}5PF_6]^{5+}$, 742.82 $[M\text{-}6PF_6]^{6+}$, 616.00 $[M\text{-}7PF_6]^{7+}$.

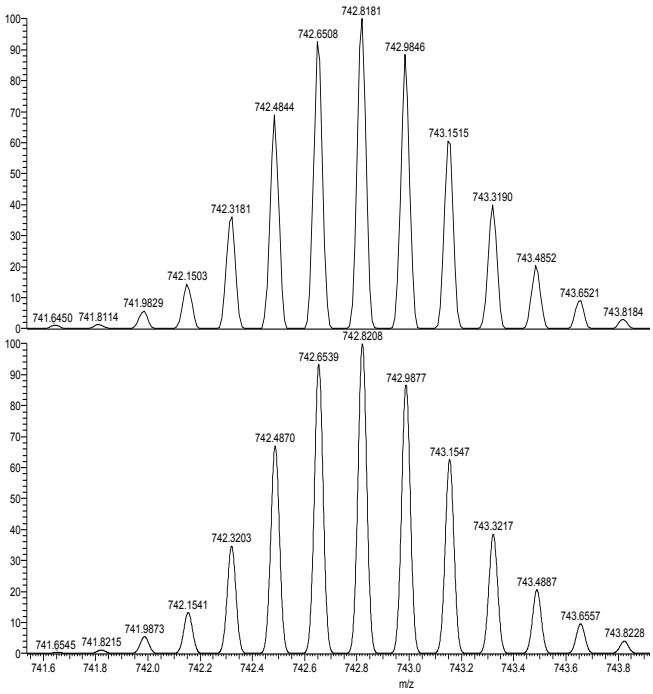

Fig. S8. HRESI-MS of $[M–6(PF_6)]^{2+}$ peak of $[Fe_4\mathbf{3}](Cl)(PF_6)_7$. Experimental spectrum (top) and calculated spectrum (bottom).

S3.5 General Procedure for the Synthesis of Knots **1-3**

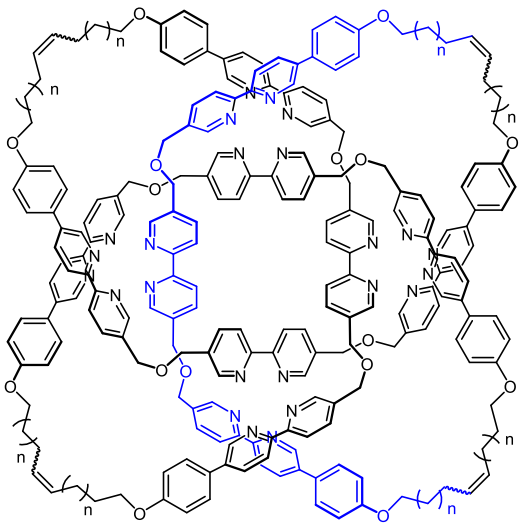

n=1, **1**; n=4, **2**; n=7, **3**

General Procedure: Metallic knots (20 mg) was dissolved in acetonitrile (4.5 mL) and warmed to 70°C in a sealed vial. Aqueous sodium hydroxide (4.5 mL, 1 M) was added and the mixture stirred at 70°C until the characteristic red colour of the complex was replaced by a grey/brown colour. The vial was cooled down to room temperature instantly and distilled water (10 mL) was added to ensure the full precipitation of any non-polar compounds formed in the reaction, which were collected by filtration onto celite. The solid was then washed with excess water and ethanol before being taken up in CH_2Cl_2. Removal of the solvent under reduced pressure gave corresponding organic knots.

Following the general procedure, the reaction of $[Fe_4\mathbf{2}](PF_6)_8$ took 10 min and **2** was isolated as beige solid (6.3 mg, 1.7 μmol) in 43% yield. The lettering corresponds to the proton labelling in ligand **L2**.

^{1}H NMR (600 MHz, $CDCl_3$) δ 8.62 – 8.57 (m, 1H, H^k), 8.49 – 8.44 (m, 2H, $H^{c,f}$), 8.21 – 8.11 (m, 3H, $H^{a,h,i}$), 7.65 – 7.54 (m, 3H, $H^{b,g,j}$), 7.32 – 7.27 (m, 2H, H^l), 6.83 – 6.74 (m, 2H, H^m), 5.42 – 5.31 (m, 1H, H^t), 4.48 – 4.37 (m, 2H, $H^{d,e}$), 3.91 – 3.80 (m, 2H, H^n), 2.06 – 1.90 (m, 2H, H^s), 1.77 – 1.66 (m, 2H, H^o), 1.45 – 1.18 (m, 6H, $H^{p,q,r}$). ^{13}C NMR (151 MHz, $CDCl_3$) δ 159.28, 155.41, 153.78, 148.60, 148.54, 147.00, 136.36, 136.30, 135.78, 134.25, 133.36, 133.08, 130.46, 129.99, 129.62, 128.02, 120.85, 120.69, 115.09, 69.93, 69.80, 68.05, 67.97, 46.32, 32.67, 29.97, 29.83, 29.21, 29.00, 27.37, 26.07, 26.01. LRESI-MS (in methanol with formic acid): *m/z* = 1859.00 $[M+2H]^{2+}$ requires 1859.83; 1239.92 $[M+3H]^{3+}$ requires 1240.22; 930.08 $[M+4H]^{4+}$ requires 930.42; 744.42 $[M+5H]^{5+}$ requires 744.53.

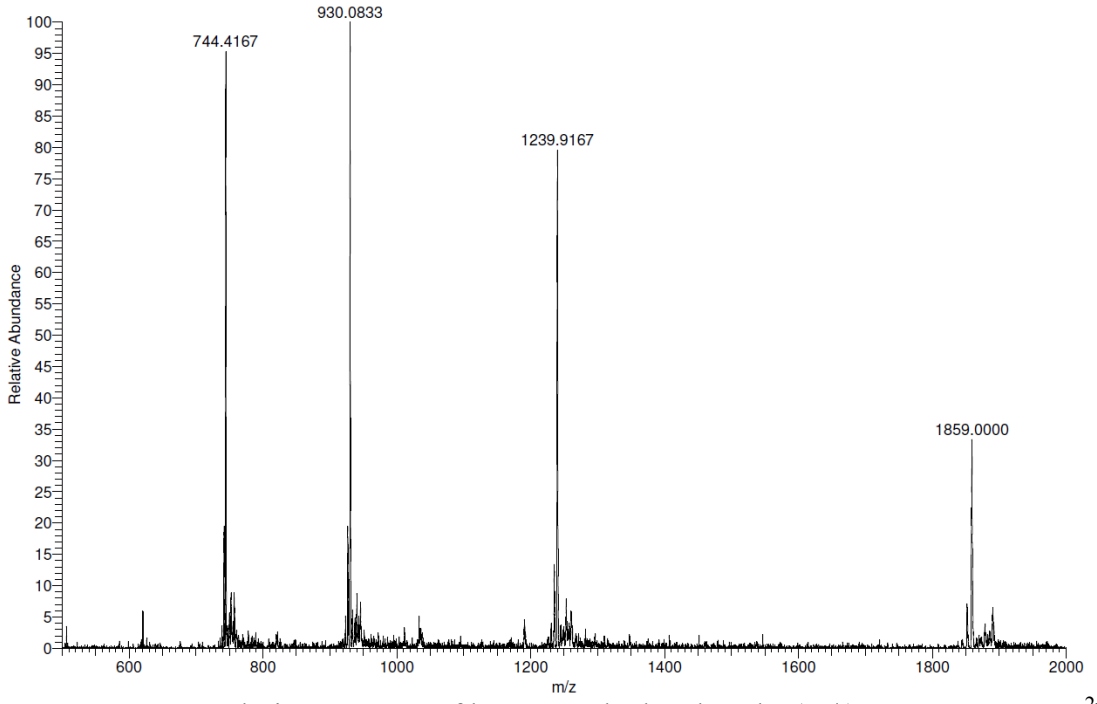

Fig. S9. Low-resolution ESI-MS of knot **2**. Calculated peaks (*m/z*) 1859.83 $[M+2H]^{2+}$, 1240.22 $[M+3H]^{3+}$, 930.42 $[M+4H]^{4+}$, 744.53 $[M+5H]^{5+}$.

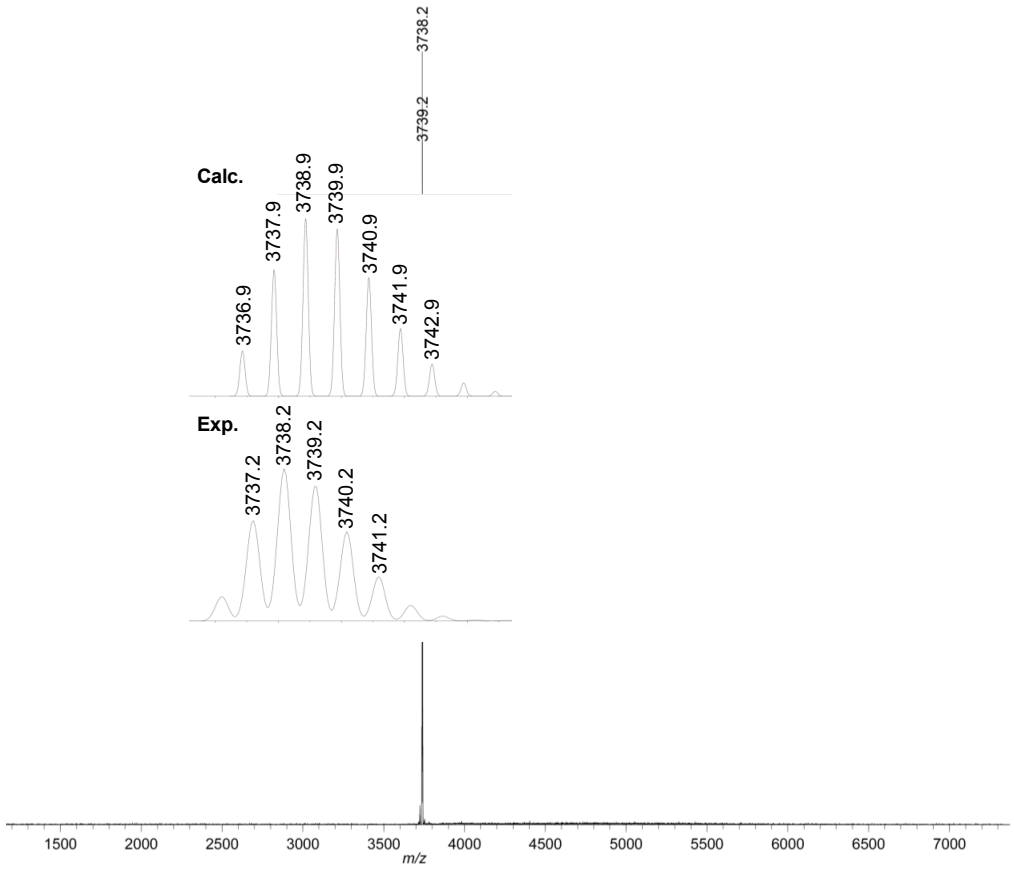

Fig. S10. MALDI-TOF spectrum of the knot **2** (calcd. for $C_{240}H_{240}N_{24}O_{16}Na^{+}$, 3738.8).

Following the general procedure, the reaction of $[Fe_4\mathbf{3}](PF_6)_8$ took less than 5 min and **3** was isolated as beige solid (9.7 mg, 2.4 μmol) in 65% yield. The lettering corresponds to the proton labelling in ligand **L3**.

^{1}H NMR (600 MHz, $CDCl_3$) δ 8.69 – 8.63 (m, 1H, H^k), 8.55 – 8.49 (m, 2H, $H^{c,f}$), 8.28 – 8.18 (m, 3H, $H^{a,h,i}$), 7.72 – 7.60 (m, 3H, $H^{b,g,j}$), 7.38 – 7.29 (m, 2H, H^l), 6.85 – 6.76 (m, 2H, H^m), 5.40 – 5.29 (m, 1H, H^v), 4.50 (s, 2H, $H^{d,e}$), 3.90 – 3.79 (m, 2H, H^n), 2.03 – 1.88 (m, 2H, H^u), 1.73 – 1.64 (m, 2H, H^o), 1.41 – 1.17 (m, 12H, $H^{p,q,r,s,t,u}$). ^{13}C NMR (151 MHz, CDCl3) δ 159.28, 155.41, 153.78, 148.60, 148.54, 147.00, 136.36, 136.30, 135.78, 134.25, 133.36, 133.08, 130.46, 129.99, 129.62, 128.02, 120.85, 120.69, 115.09, 69.93, 69.80, 68.05, 67.97, 46.32, 32.67, 29.97, 29.83, 29.21, 29.00, 27.37, 26.07, 26.01. LRESI-MS (in methanol with formic acid): *m/z* = 2027.09 $[M+2H]^{2+}$ requires 2027.64; 1351.00 $[M+3H]^{3+}$ requires 1352.00; 1013.27 $[M+4H]^{4+}$ requires 1014.32; 810.45 $[M+5H]^{5+}$ requires 811.44; 675.10 $[M+5H]^{5+}$ requires 676.55.

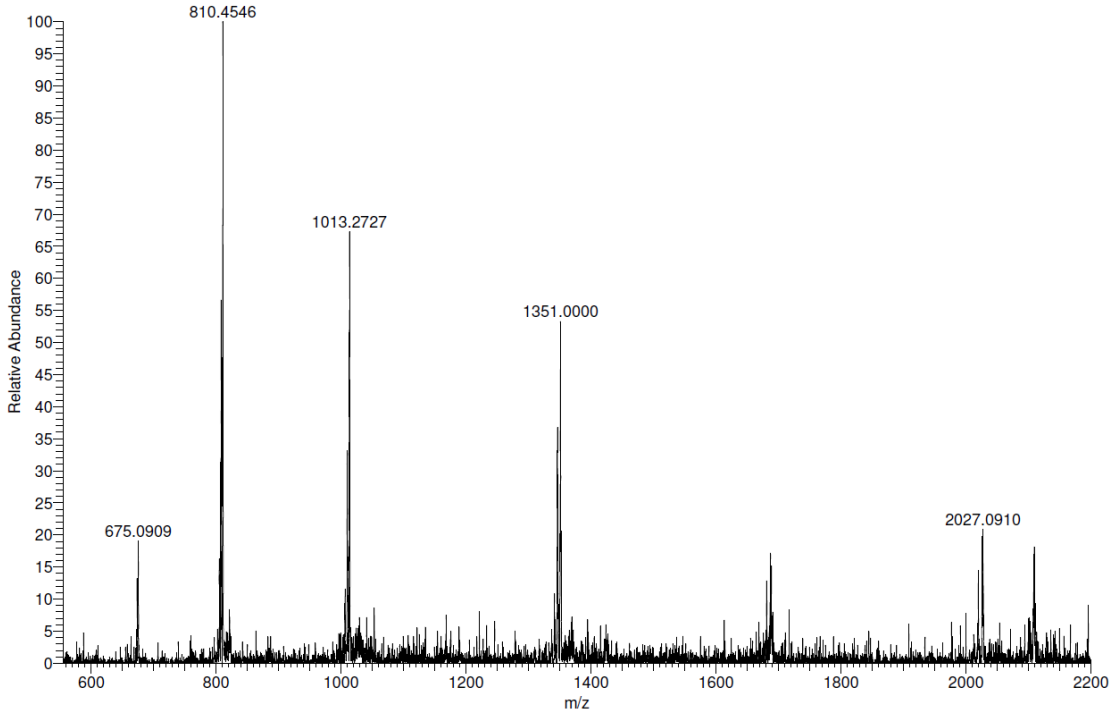

Fig. S11. Low-resolution ESI-MS of knot **3**. Calculated peaks (*m/z*) 2027.64 $[M+2H]^{2+}$, 1352.00 $[M+3H]^{3+}$, 1014.32 $[M+4H]^{4+}$, 811.44 $[M+5H]^{5+}$, 676.55 $[M+6H]^{6+}$.

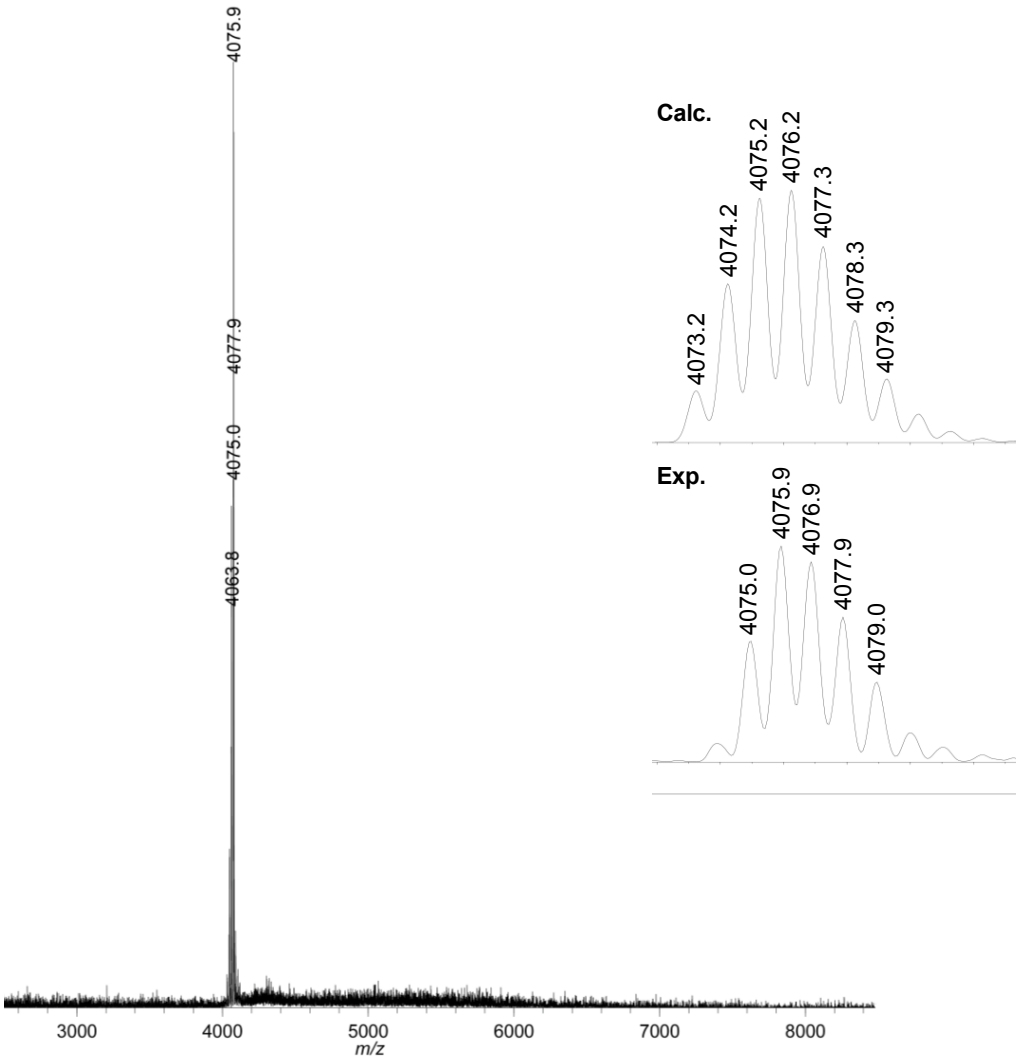

Fig. S12. MALDI-TOF spectrum of the knot **3** (calcd. for $C_{264}H_{288}N_{24}O_{16}Na^{+}$, 4076.2).

S4. NMR Spectra

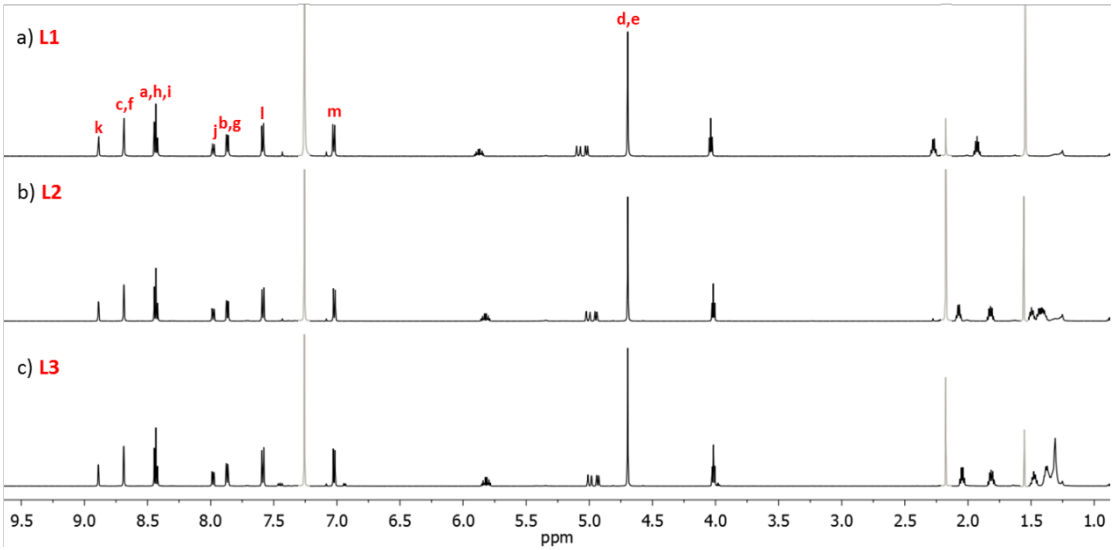

Fig. S13. ^{1}H NMR spectra (600 MHz, $CDCl_3$, 298K) of ligands (a) **L1**; (b) **L2** and (c) **L3**. The lettering corresponding to the proton labelling in Scheme S1.

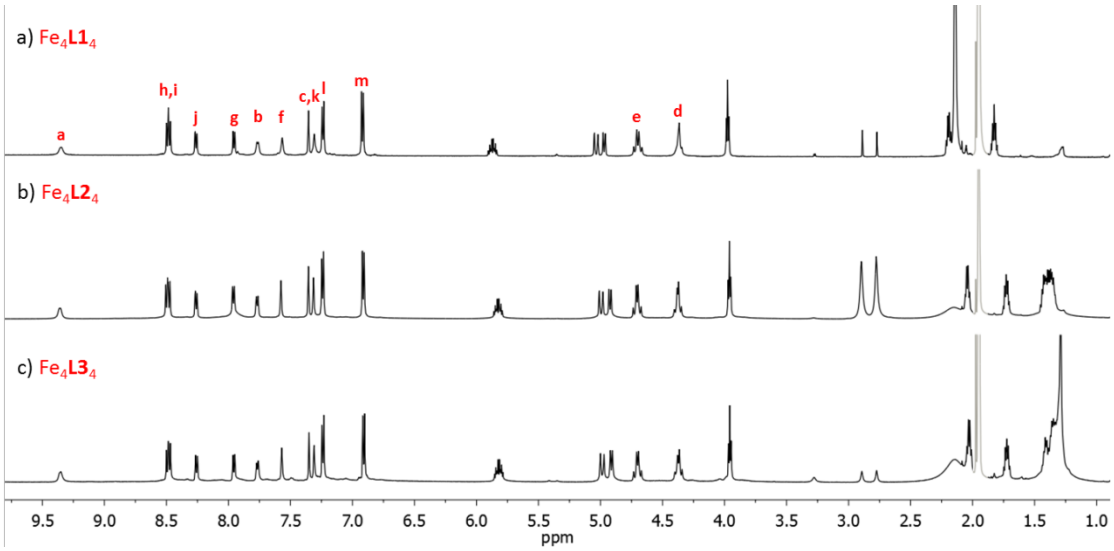

Fig. S14. ^{1}H NMR spectra (600 MHz, CD_3CN, 298K) of circular helicates (a) $[Fe_4\mathbf{L1}_4](PF_6)_8$; (b) $[Fe_4\mathbf{L2}_4](PF_6)_8$ and (c) $[Fe_4\mathbf{L3}_4](PF_6)_8$. The lettering corresponding to the proton labelling in Scheme S1.

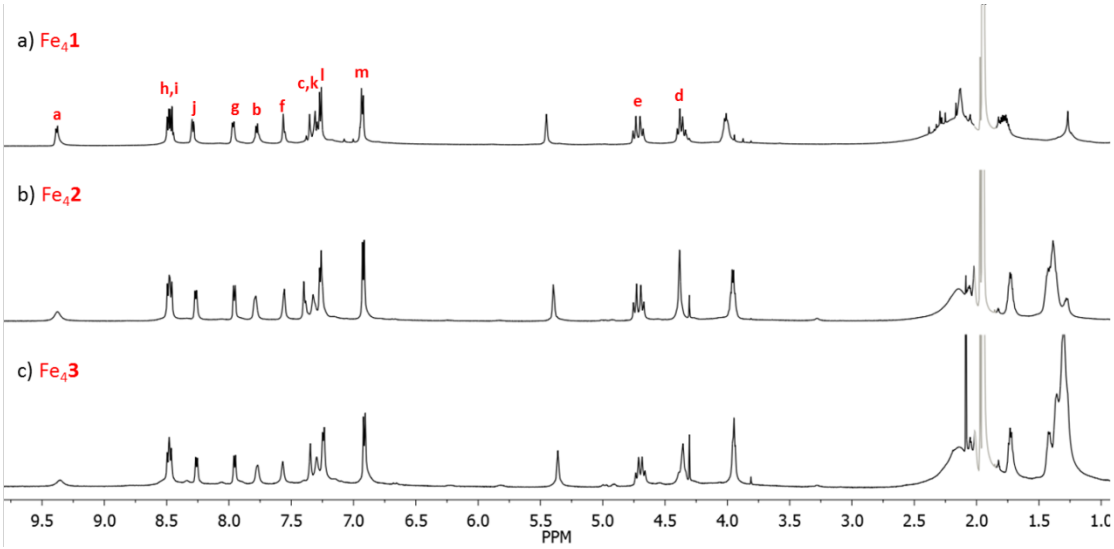

Fig. S15. ^{1}H NMR spectra (600 MHz, CD_3CN, 298K) of metallic knots (a) [Fe_4**1**]$(PF_6)_8$; (b) [Fe_4**2**]$(PF_6)_8$ and (c) [Fe_4**3**]$(PF_6)_8$. The lettering corresponding to the proton labelling in Scheme S1.

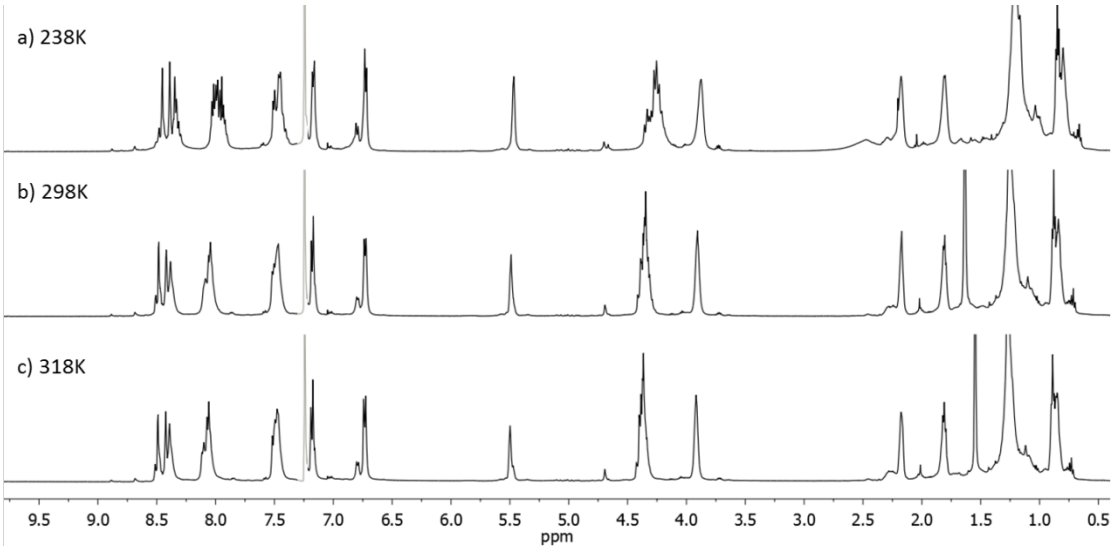

Fig. S16. Variable Temperature ^{1}H NMR spectra (600 MHz, $CDCl_3$) of knot **1** (a) 238K; (b) 298K and (c) 318K.

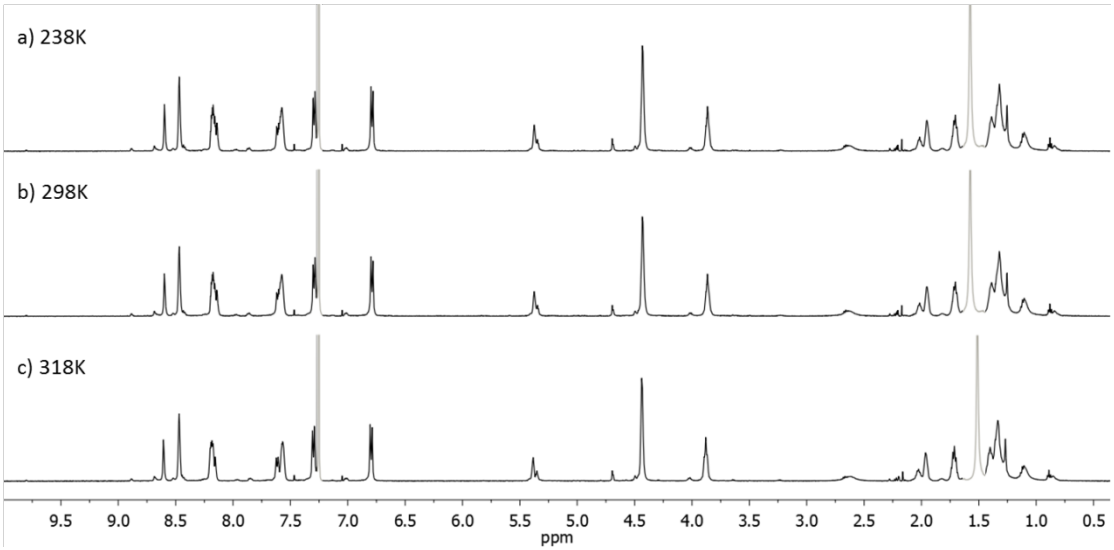

Fig. S17. Variable Temperature ^{1}H NMR spectra (600 MHz, $CDCl_3$) of knot **2** (a) 238K; (b) 298K and (c) 318K.

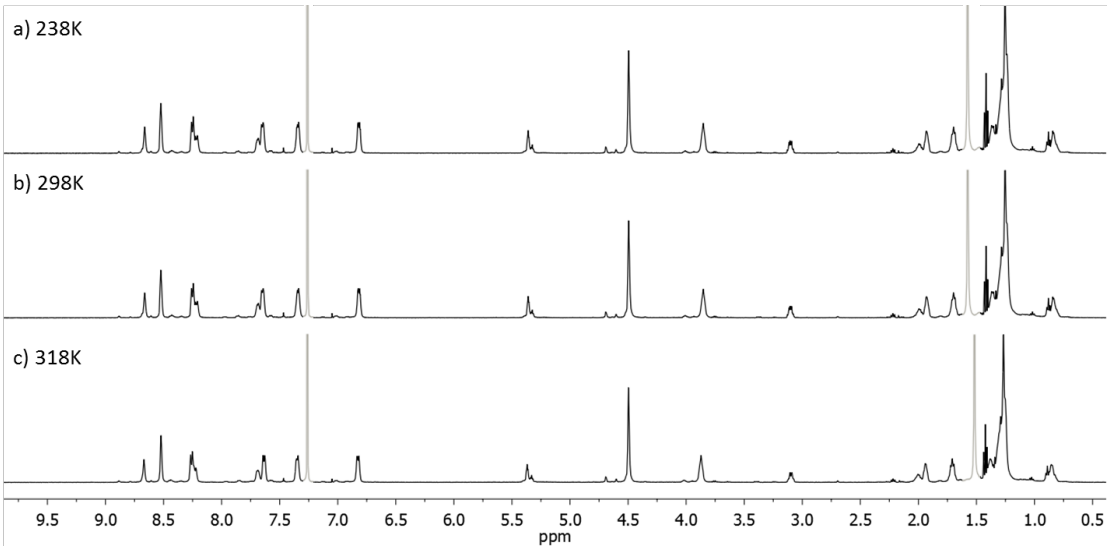

Fig. S18. Variable Temperature ^{1}H NMR spectra (600 MHz, $CDCl_3$) of knot **3** (a) 238K; (b) 298K and (c) 318K.

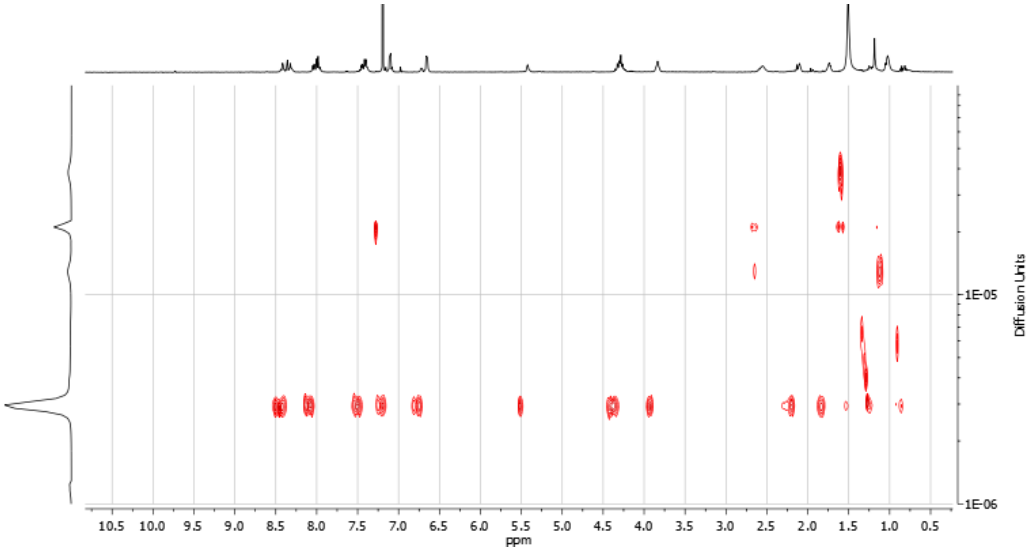

Fig. S19. DOSY NMR spectra (500 MHz, $CDCl_3$, 298K) of knot **1**, $D = 2.9\ m^2\ s^{-1}\ x\ 10^{-10}$.

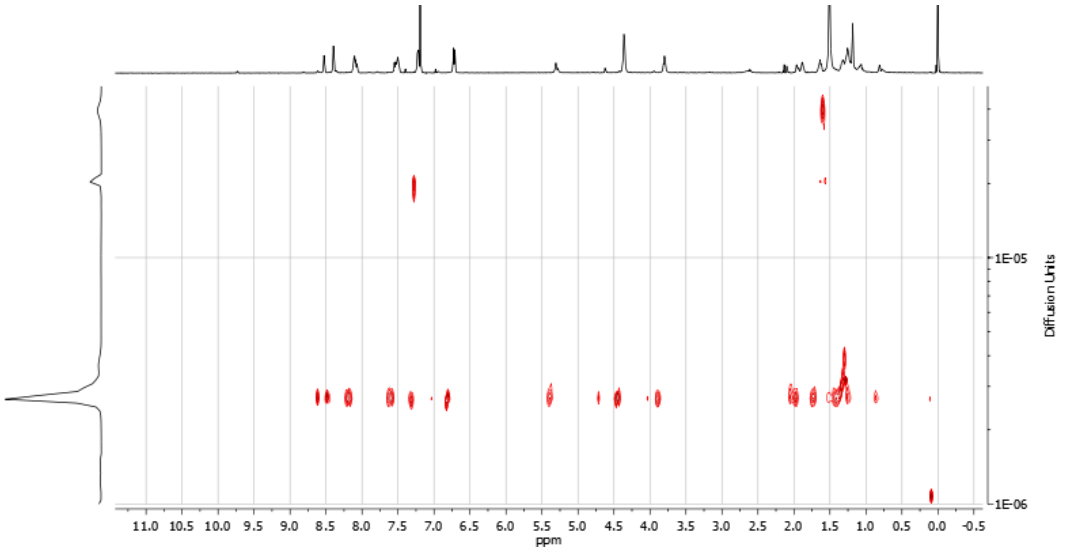

Fig. S20. DOSY NMR spectra (500 MHz, $CDCl_3$, 298K) of knot **2**, $D = 2.7\ m^2\ s^{-1}\ x\ 10^{-10}$.

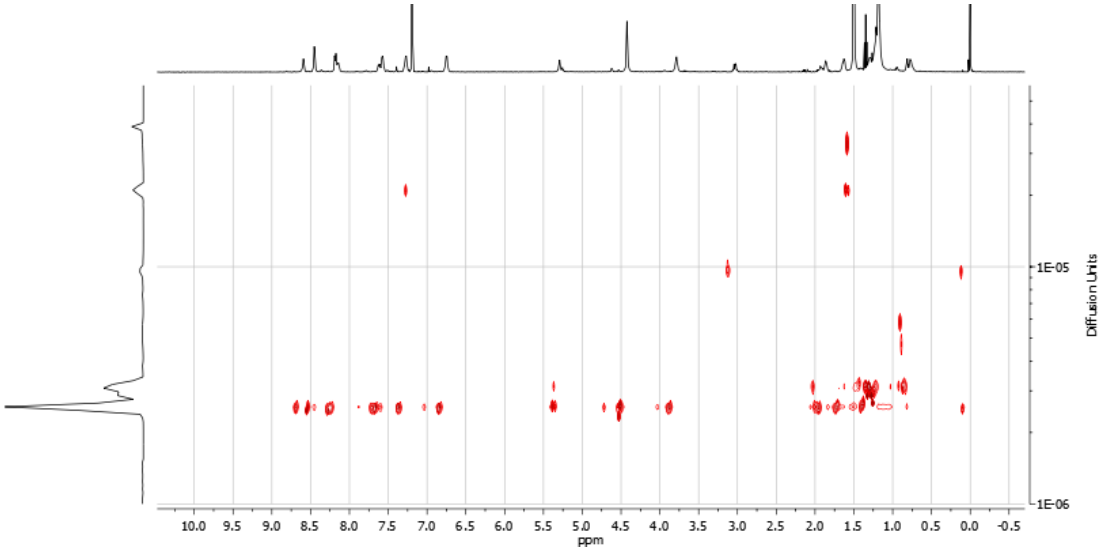

Fig. S21. DOSY NMR spectra (500 MHz, $CDCl_3$, 298K) of knot **3**, D = 2.5 m^2 s^{-1} x 10^{-10}.

Table S1. Proton signals in three metallated knots and organic knots. The alkene protons (H^q in **1**, H^t in **2**, H^v in **3**) and allylic protons (H^p in **1**, H^s in **2**, H^u in **3**) are labeled in red due to the different labeling in three knots. It is clear that the protons are placed in similar chemical environments in the metallated knot but are changed after removing the metal templates.

H / Knot (ppm)	**$Fe_4$1**	**$Fe_4$2**	**$Fe_4$3**	H / Knot (ppm)	**1**	**2**	**3**
H^a	9.38	9.38	9.36	H^k	8.48	8.60	8.66
H^h	8.49	8.49	8.49	$H^{c,f}$	8.41	8.47	8.53
H^i	8.47	8.47	8.47	$H^{a,i}$	8.09	8.18	8.25
H^j	8.28	8.27	8.26	H^h	8.05	8.15	8.22
H^g	7.96	7.96	7.96	H^j	7.51	7.61	7.69
H^b	7.78	7.79	7.78	$H^{g,b}$	7.47	7.58	7.65
H^f	7.57	7.56	7.57	H^l	7.18	7.29	7.34
H^m	6.93	6.92	6.92	H^m	6.73	6.79	6.82
$H^{(CH-CH)}$	5.45	5.40	5.36	$H^{(CH-CH)}$	5.49	5.36	5.34
H^e	4.71	4.71	4.70	$H^{d,e}$	4.35	4.43	4.50
H^d	4.37	4.38	4.36	H^n	3.90	3.86	3.84
H^n	4.00	3.96	3.96	H^o	1.81	1.70	1.69
				$H^{(CH-CH-CH2)}$	2.18	1.95	1.93

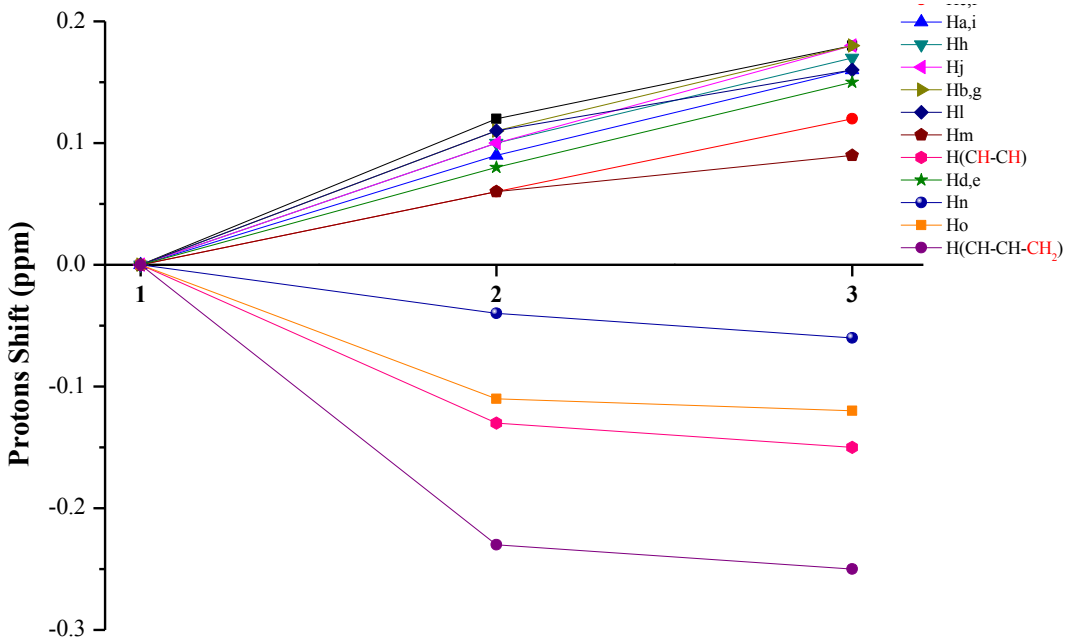

Fig. S22. Protons shift trends of the three organic knots. The proton signals in knot **1** are set up to 0 as standard (Table S1). It is clear that the aromatic protons shift to low field gradually (*positive value*) and the alkyl protons shite to high field gradually (*negative value*), which indicate the generation of fewer π-π interactions and more CH-π interactions during loosening the knots.

S5. Chiral HPLC resolution of demetallated knots

The racemic mixtures of knots were separated by passing a solution of knots in CH_2Cl_2 (10 mg / 1.5 mL) over a semi-preparative Chiralpak® IF HPLC column with an eluent of n-Heptane/THF/Diethylamine (50:50:0.1) twice and the purity of the enantioisomers were further determined by passing a solution of knots in CH_2Cl_2 (1 mg / 1.5 mL) over an analytic Chiralpak® IF HPLC column with an eluent of n-Heptane/THF/Diethylamine (55:45:0.1).

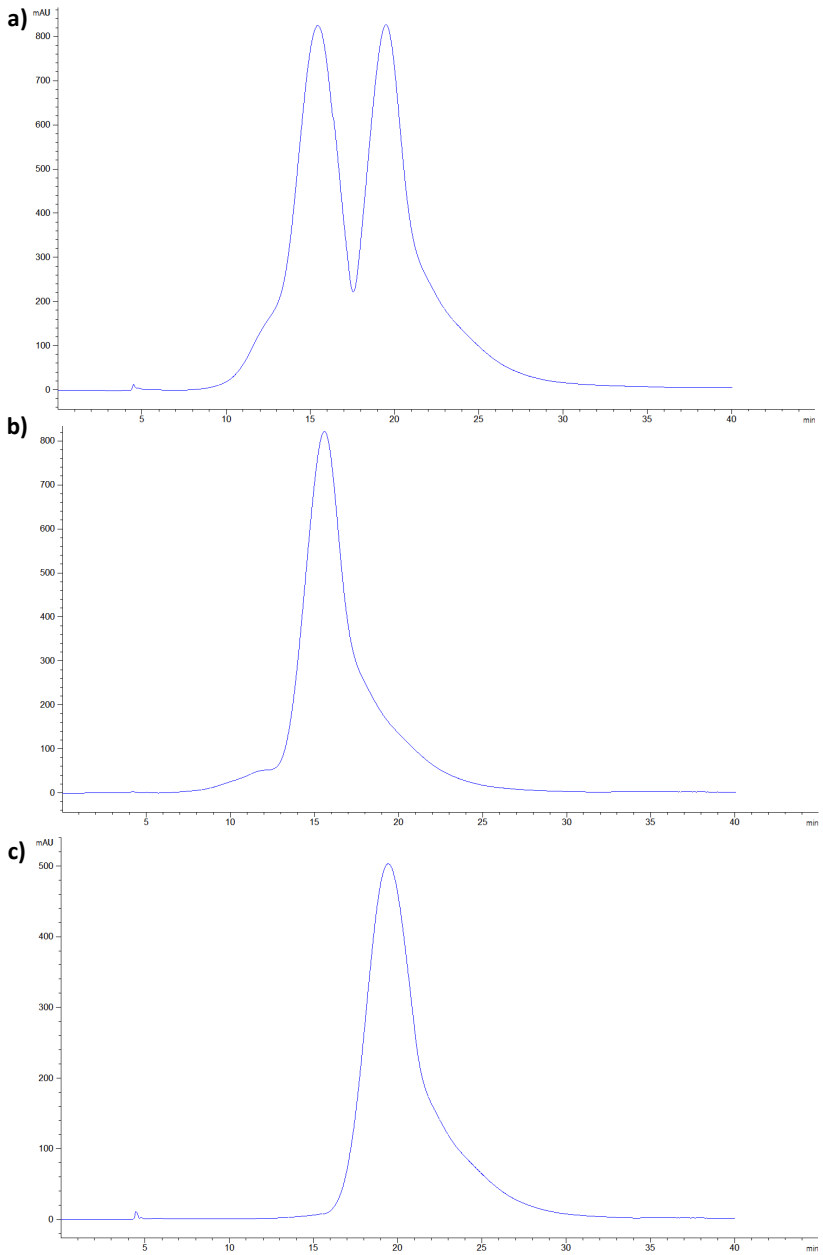

Fig. S23. Chiral HPLC trace of a) the racemic mixture of demetallated knot **2**; b) the (+)-**2** sample and c) (-)-**2** sample.

(+)-**2** sample (t = 15.59 min, ee 95% determined by chiral HPLC)
Measured $[a]_D^{25}$ = +15.5 (c = 2.5 mg/ml in CH_2Cl_2)
Corrected $[a]_D^{25}$ = +16.3 (c = 2.5 mg/ml in CH_2Cl_2)
(-)-**2** sample (t = 19.42 min, ee 100 determined by chiral HPLC)
$[a]_D^{25}$ = -17.2 (c = 2.5 mg/ml in CH_2Cl_2)
Separation factor is 1.39

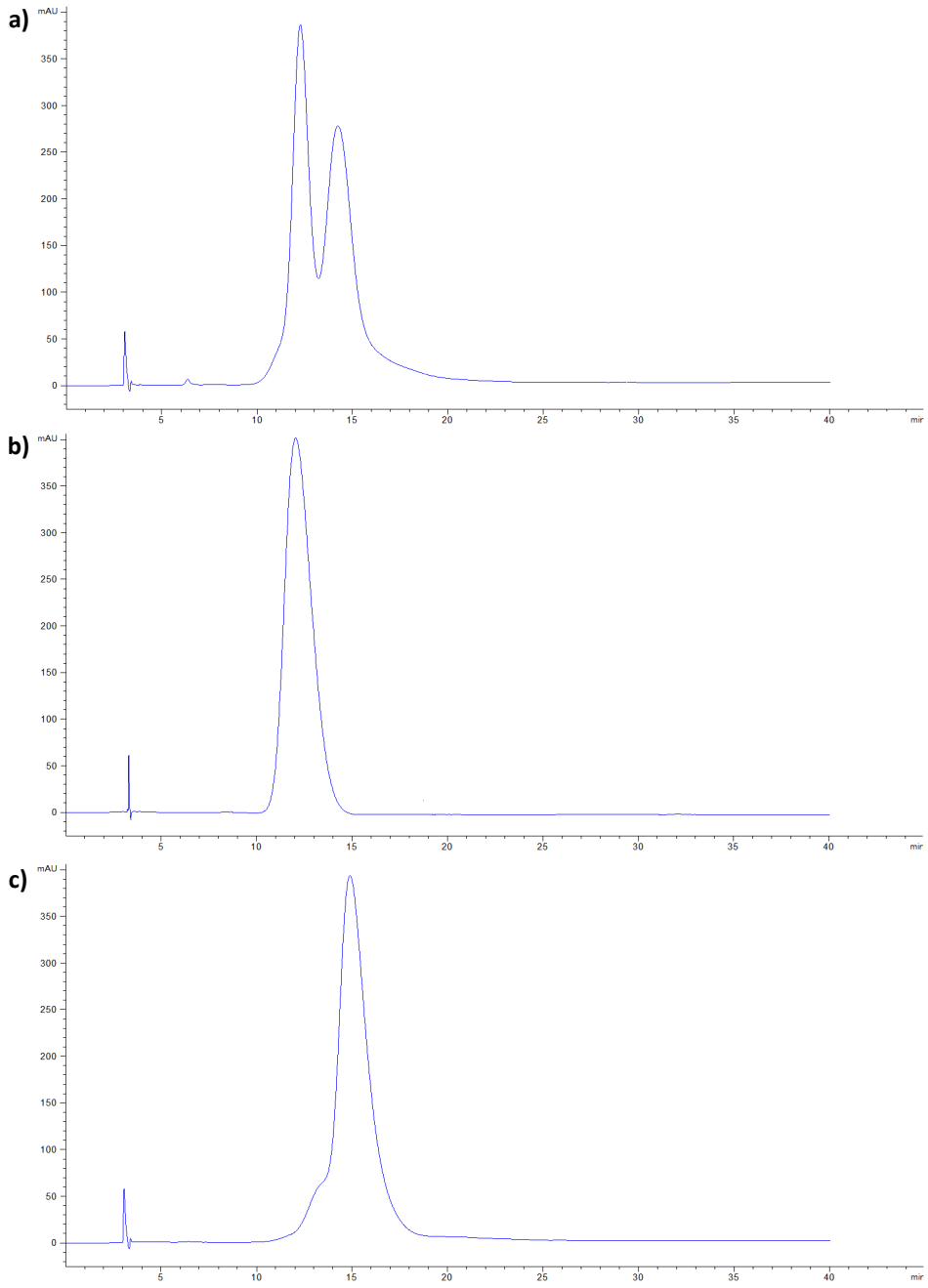

Fig. S24. Chiral HPLC trace a) the racemic mixture of demetallated knot **3**; b) the (+)-**3** sample and c) (-)-**3** sample.

(+)-**3** sample (t = 12.09 min, ee 100% determined by chiral HPLC)
$[a]_D^{25}$ = +15.3 (c = 2.5 mg/ml in CH_2Cl_2)
(-)-**3** sample (t = 14.91 min, ee 90 determined by chiral HPLC)
Measured $[a]_D^{25}$ = -13.6 (c = 2.5 mg/ml in CH_2Cl_2)
Corrected $[a]_D^{25}$ = -15.1 (c = 2.5 mg/ml in CH_2Cl_2)
Separation factor is 1.19

S6. UV-Vis Spectra

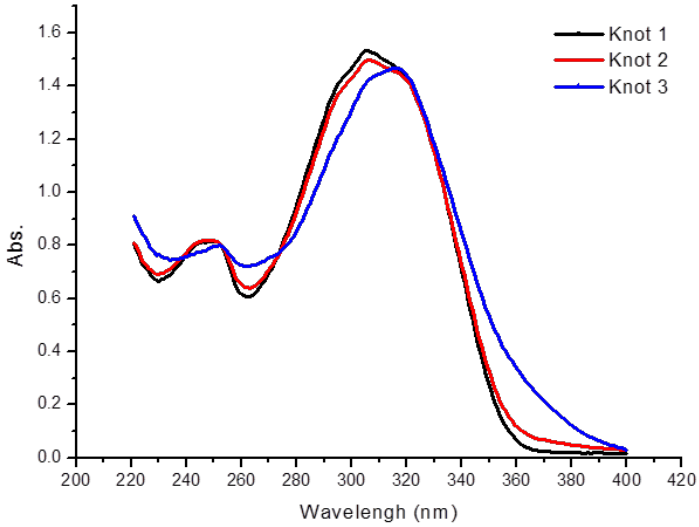

Fig. S25. UV-Vis absorption spectra of demetallated knots **1-3** (1.78×10^{-4} M in CH_2Cl_2).

S7. Tandem Mass Spectra

The demetalated knots **1-3** were dissolved in CH_2Cl_2 with formic acid added to generate multiply protonated ions. The collision induced dissociation (CID) experiments were conducted on 2^+ species for all knots and the energy of CID gradually increased (1 ev / step) until the fragments can be detected. The charge of each peak is demonstrated by zoomed spectra.

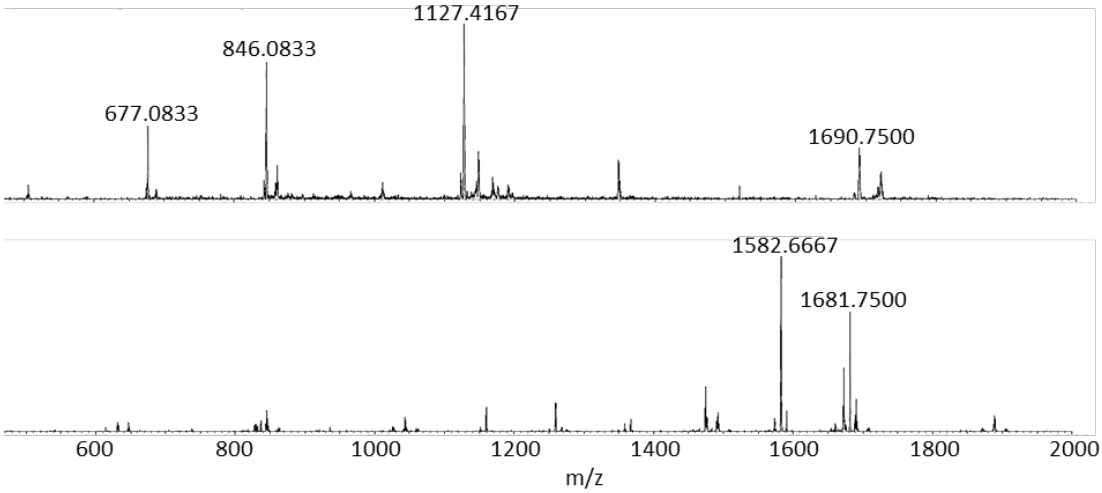

Fig. S26. LRESI-MS (*top*) and MS-MS (*bottom*) of $[M+2H]^{2+}$ peak (*m/z* = 1690.75, width 1 unit) from the demetalated knot **1** (CID = 28 ev).

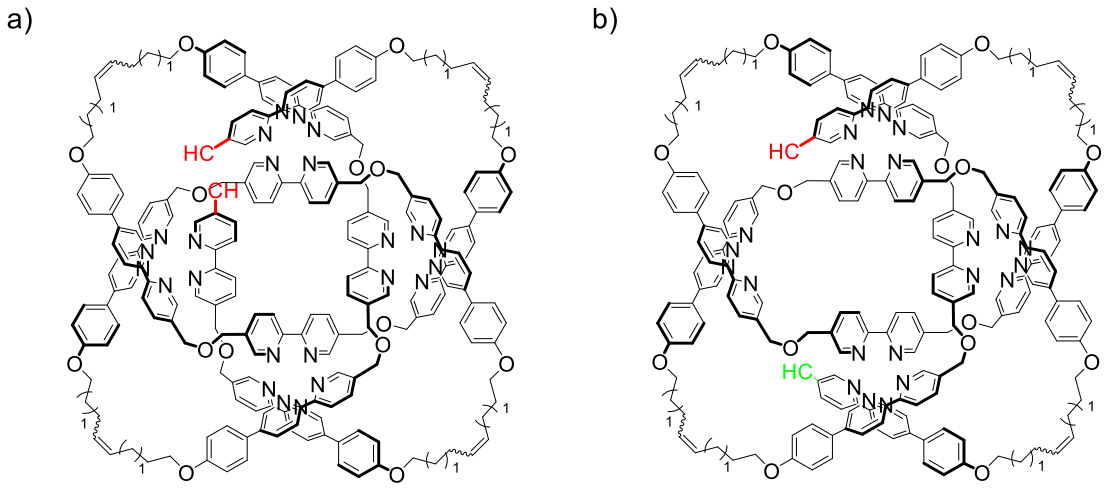

Scheme S3. The structures of fragments formed under MS-MS experiment of **1**. The broken bonds were labeled by colors. Calculated peak (*m/z*) for *type 1* fragmentation a) [**1**-H_2O+2H]$^{2+}$: 1681.75; b) [**1**-$C_{12}H_{12}N_2O_2$+2H]$^{2+}$: 1582.71. Only *type 1* fragmentation was observed in knot **1**.

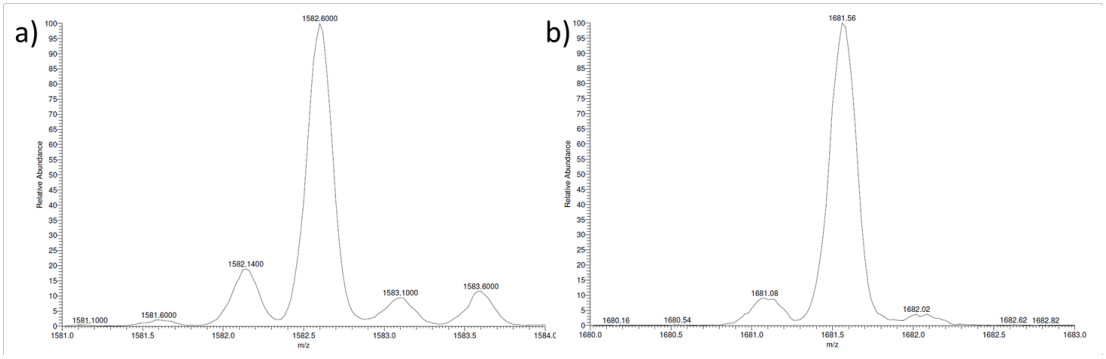

Fig. S27. LRESI-MS zoom scan of the peaks displayed in Fig. S26 determining the charge of each peak allowing the assignment of the different species. (a) $[M]^{2+}$ species; (b) $[M]^{2+}$ species.

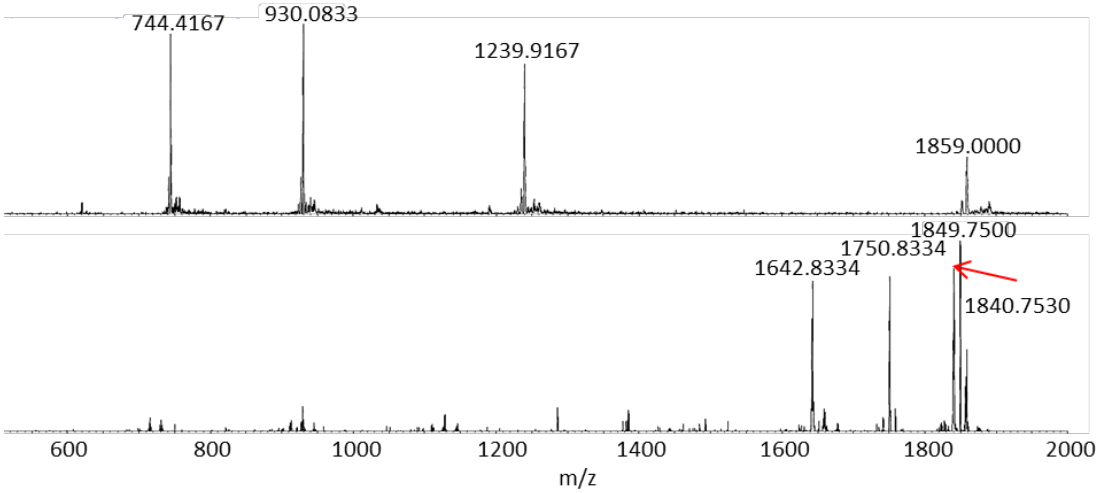

Fig. S28. LRESI-MS (*top*) and MS-MS (*bottom*) of $[M+2H]^{2+}$ peak (*m/z* = 1859.00, width 1 unit) from the demetalated knot **2** (CID = 35 ev).

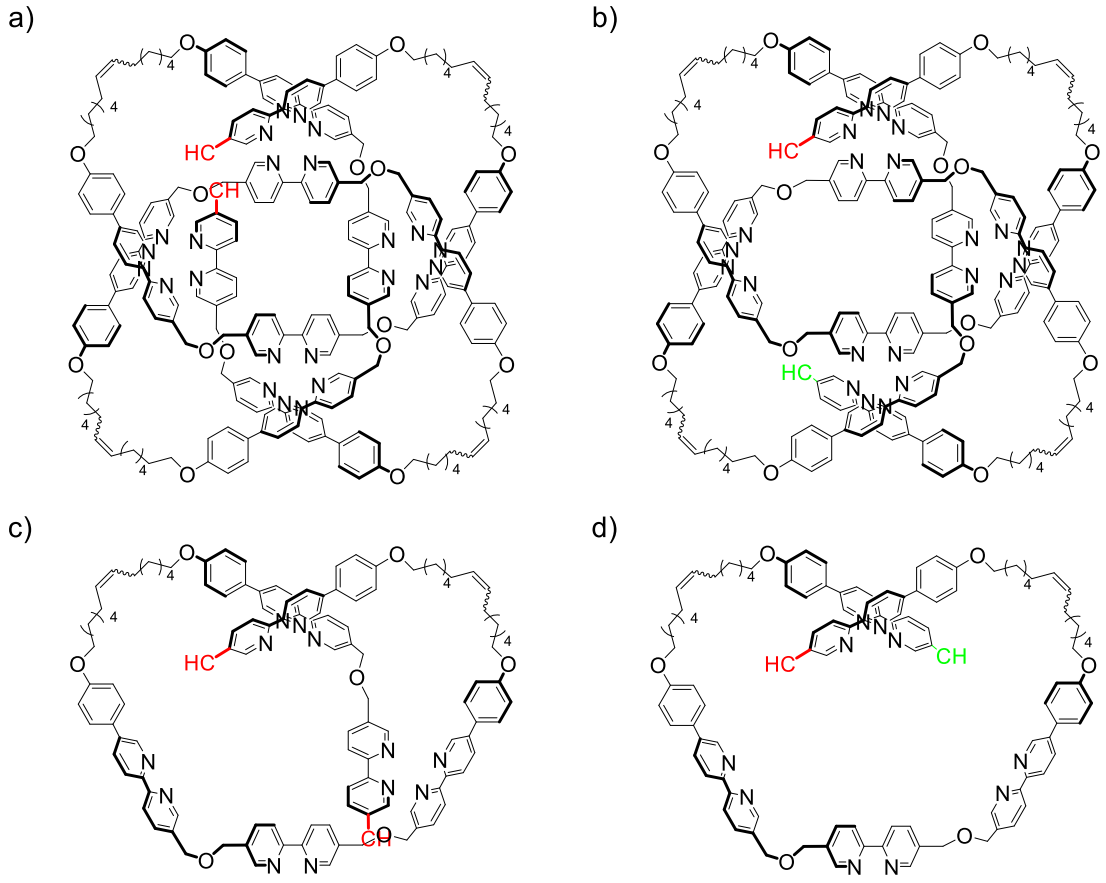

Scheme S4. The structures of fragments formed under MS-MS experiment of **2**. The broken bonds were labeled by colors. Calculated peak (*m/z*) for *type 1* fragmentation a) [**2**-H_2O+2H]$^{2+}$: 1849.94; b) [**2**-$C_{12}H_{12}N_2O_2$+2H]$^{2+}$: 1750.90; and *type 2* fragmentation c) [**2**-$C_{120}H_{122}N_{12}O_9$+H]$^{+}$: 1840.94; d) [**2**-$C_{132}H_{132}N_{14}O_{10}$+H]$^{+}$: 1642.86. Both *type 1* and *type 2* fragmentations were observed in knot **2**.

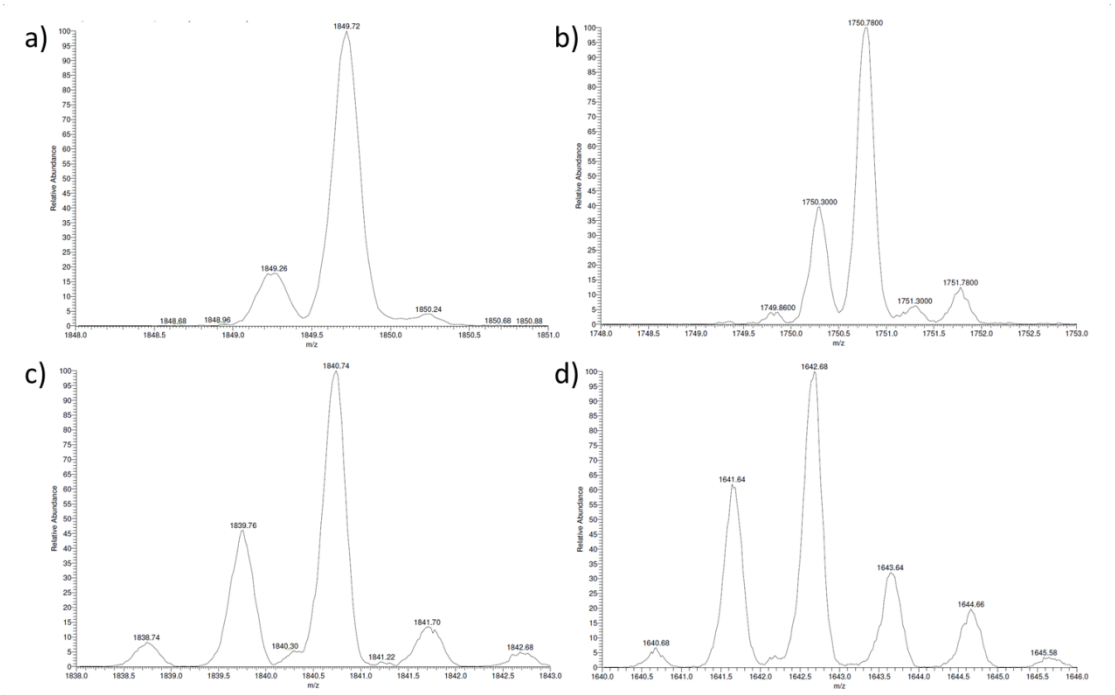

Fig. S29. LRESI-MS zoom scan of the peaks displayed in Fig. S28 determining the charge of each peak allowing the assignment of the different species. (a) $[M]^{2+}$ species; (b) $[M]^{2+}$ species; (c) $[M]^{+}$ species; (d) $[M]^{+}$ species.

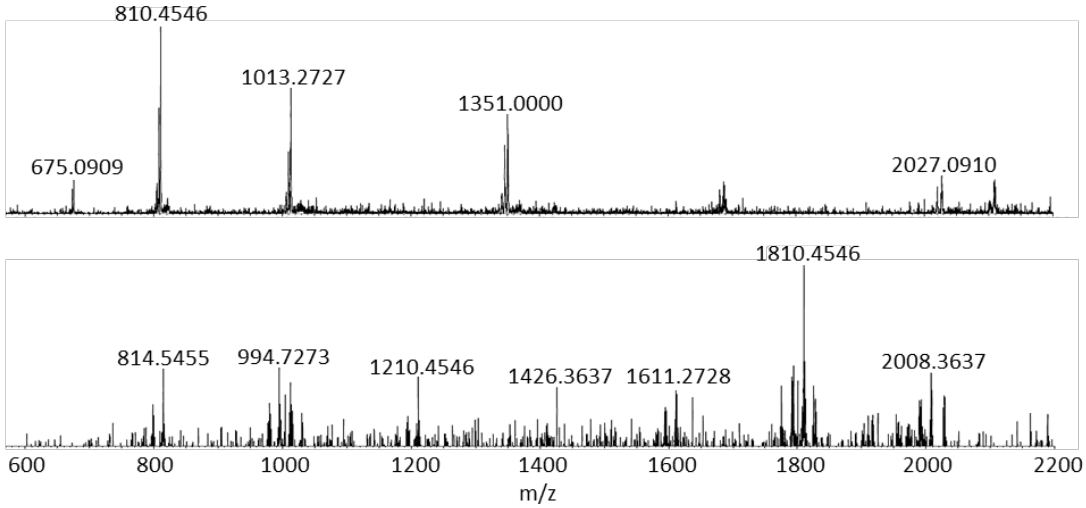

Fig. S30. LRESI-MS (*top*) and MS-MS (*bottom*) of $[M+2H]^{2+}$ peak (*m/z* = 2027.09, width 1 unit) from the demetalated knot **3** (CID = 55 ev).

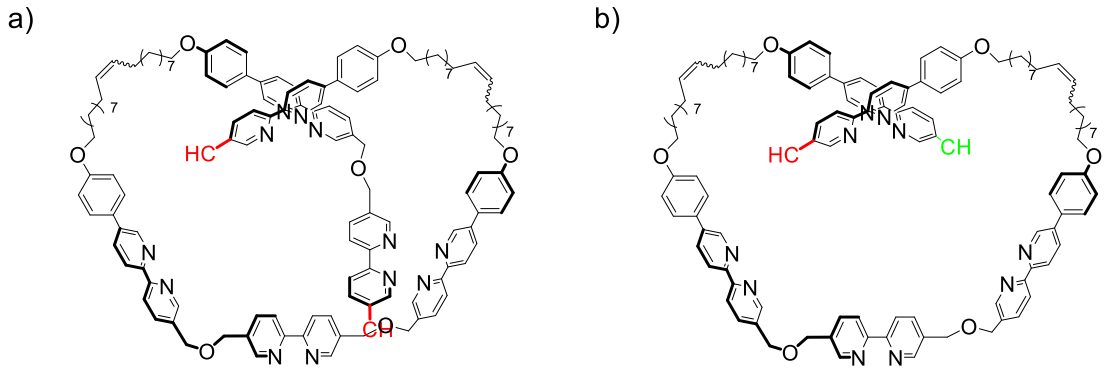

Scheme S5. The structures of fragments formed under MS-MS experiment of **3**. The broken bonds were labeled by colors. Calculated peak (*m/z*) for *type 2* fragmentation a) [**3**-$C_{132}H_{146}N_{12}O_9$+H]$^+$: 2009.12; b) [**3**-$C_{132}H_{146}N_{12}O_9$+H]$^+$: 1811.04. Only *type 2* fragmentation was observed in knot **3**.

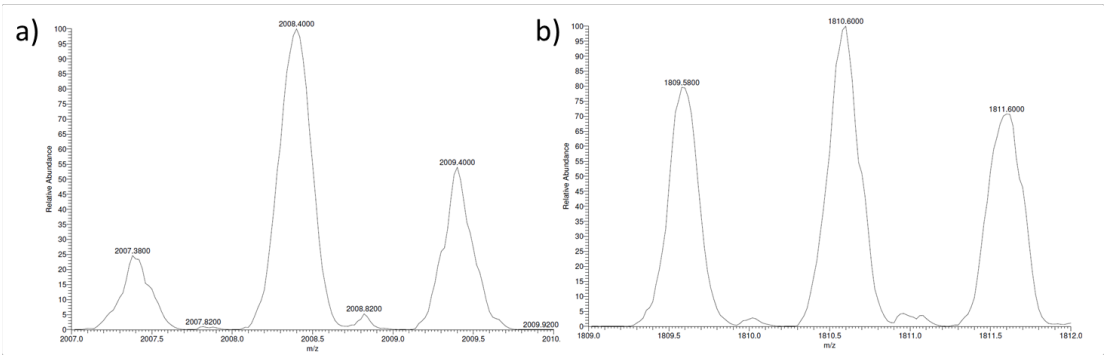

Fig. S31. LRESI-MS zoom scan of the peaks displayed in Fig. S30 determining the charge of each peak allowing the assignment of the different species. (a) $[M]^+$ species; (b) $[M]^+$ species.

S8. Computational Information

S8.1 Methods:

Molecular Dynamics Simulations. Molecular dynamics simulations were carried out with the AMBER 12.0 suite of programs.[2] The knots are parametrized using GAFF (general AMBER force field) force field[3] and the standard RESP procedure is carried out to assign charges to atoms by Antechamber).[4] The crystallographic structure of metallated knot $[Fe_4\mathbf{1}]^{8+}$ is used as starting structure for **1** and as template for building **2** and **3**. The starting structures are immersed in a solvent box of explicit $CDCl_3$ molecules. Periodic boundary conditions were used. An equilibration protocol consisting of four individual steps was applied, resulting in an unconstrained well-tempered NPT ensemble at target conditions. A Langevin thermostat was used to set a constant temperature at 298 K and 1 atm. Particle Mesh Ewald[5] summation was used throughout (cut off radius of 10 Å for the direct space sum). Bonds involving H atoms were constrained using the SHAKE algorithm,[6] and a time step of 2 fs was applied in all runs. Overall sampling time for MD production was 1 μs. Snapshot structures were saved into individual trajectory files every 5000 time steps, that is, every 10 ps of molecular dynamics, for a total of 100000 snapshots. MD simulations were carried out using pmemd. VMD was used to visualize the trajectory.[7] Two-dimensional free-energy profiles for the knots in explicit solvent were obtained as a function of PCA1 and PCA2. The program "ptraj"[2] in the AMBER package was used in the PCA. The values are given in normalized energy. The energy landscape of the peptide is visualized by means of free-energy functions, which are projected as contour lines onto a two-dimensional space formed by the PCA1/PCA2 axes. These coordinates are derived from a principal component analysis.[8] The free-energy change associated with the passage between two different states of a system in thermodynamic equilibrium is given by $\Delta G = -RT$ (ln p1/p2). Here, R is the ideal gas constant, T is the absolute temperature, and pi is the probability of finding the system in state i. The two-dimensional space defined by the PCA1 and PCA2 axes has been divided into a grid and the free energy has been calculated for each bin of the grid on the basis of the previous equation. The whole set of G values was in such a way that the lowest value (more populated bid) of the free energy surface corresponds to zero and the less populated to 1. Thus, the reported ΔG values represent the transfer free energies with respect to the bin that has been set to zero. To obtain the p values, the trajectory at ambient temperature was projected onto the PCA1/PCA2 space, and p corresponds to the number of times the trajectory "visits" a given bin.

TD-DFT calculations, at the M062X/6-31G* level of theory[9], with Gaussian09 suite of programs,[10] were run on isolated single chromophoric units, rigidly extracted from different MD knot structures selected from a PCA distribution, for **1**, **2** and **3**. MD snapshots were selected from different regions of the PCA distributions, producing two conformational sets of structures for **2** and **3**, and a single set for knot **1** (see below).

The calculated vertical electronic excitations for all chromphores, together with their oscillator strengths, were summed and convoluted with a Gaussian function (FWHM=0.15 eV) to obtain the absorption spectrum of each structure for comparison with experimental data. TD-DFT calculations were run both in gas phase and in solution (CH_2Cl_2), by means of the CPCM polarizable conductor model,[11] with the Pauling cavity set.

In order to understand the two different CID fragmentation pathways experimentally found, we used Wiberg Bond Indices (WBIs) analysis as implemented in Gaussian 09 suite of programs on double charged **1** and **3.** The WBI analysis allows to provide a relative scale of bond strengths to predict bonds mostly likely to break.

S8.2 Molecular Dynamics

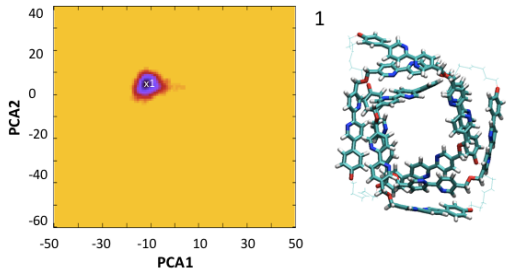

Fig. S32. Left: FES of **1,** the small white cross corresponds to the representative structure on the right. Right: Snapshot of thermally equilibrated **1**. Solvent molecules removed for clarity. The alkyl chains (flexible part) are depicted as sticks, the aromatic motifs (rigid part) are displayed as thick rods.

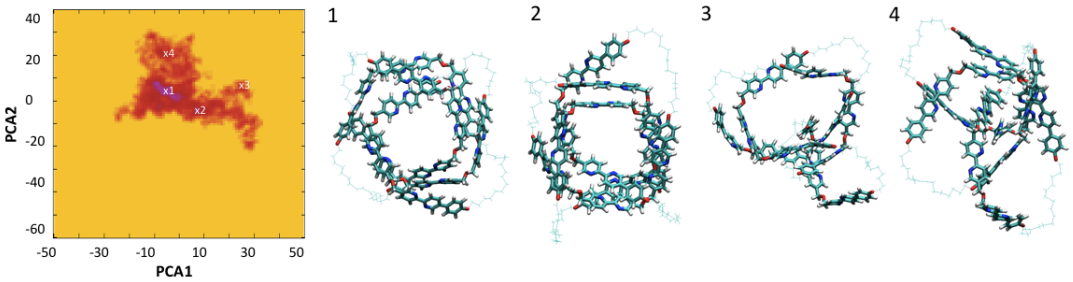

Fig. S33. Left: FES of **2,** the small white crosses correspond to the representative structures on the right. Right: Snapshots of thermally equilibrated **2**. Solvent molecules removed for clarity. The alkyl chains (flexible part) are depicted as sticks, the aromatic motifs (rigid part) are displayed as thick rods.

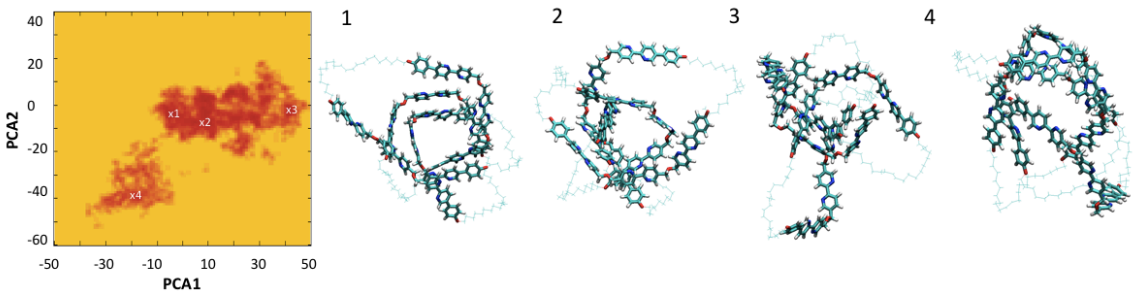

Fig. S34. Left: FES of **3**, the small white crosses correspond to the representative structures on the right. Right: Snapshots of thermally equilibrated **3**. Solvent molecules removed for clarity. The alkyl chains (flexible part) are depicted as sticks, the aromatic motifs (rigid part) are displayed as thick rods.

S8.3 Absorption spectra

Time Dependent Density Functional Theory calculations were performed on all the chromophores of **1**, **2**, and **3** as taken from the Molecular Dynamics simulations. The calculations were carried out both in the vacuum and in CH_2Cl_2. The intent was to ascertain whether the effect observed experimentally could be qualitatively accounted for by the calculations.

Fig. S35 (top) shows the calculated spectra for a number of structures taken around the global minimum of **1**. Even the reduced conformational dynamics of this knot introduces spectral variations. The overall effect is a broadening of the spectra. The solvent shifts to higher wavenumbers the spectra. Fig. S35 (center) shows the calculated spectra for a number of structures taken around the global minimum of **2** and other local minimum structures. The conformational dynamics of the knot introduces spectral variations that are enhanced with respect to **1**. Fig. S35 (bottom) shows the effect is even more marked for **3**.

In all spectra, the bipyridine unit is responsible for the lower wavelength peaks, around 260-270 nm, while, the phenyl-bipyridine units contribute with higher wavelength bands, around 280-310 nm.

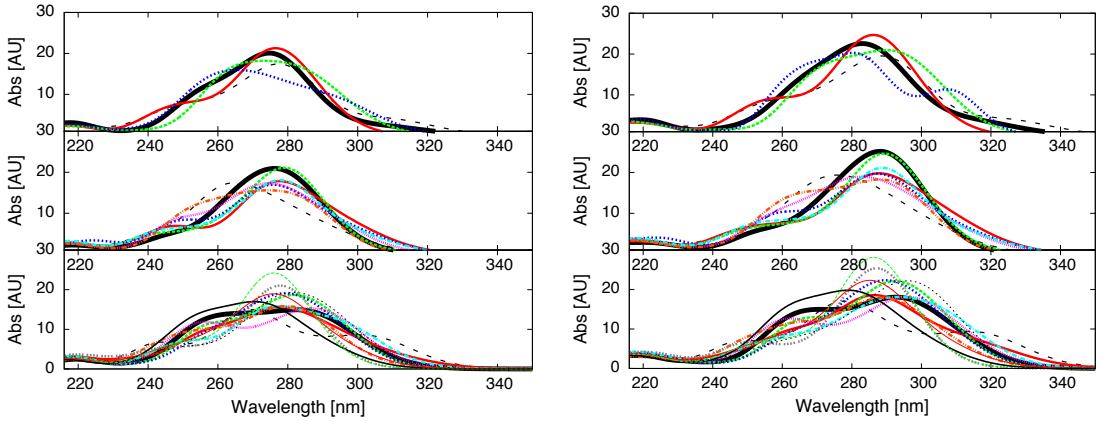

Fig. S35. Calculated absorption spectra of several low-energy structures of **1** (*top*), **2** (*center*) and **3** (*bottom*). Left: vacuum, Right: CH_2Cl_2.

These calculations were taken as indicative of the fact the structures obtained by the Molecular Dynamics simulations are able to generate spectra where shifts of the transitions are present.

The chromophores of the knots that generate the lower energy bands are the phenyl-bipyridine units, which are characterized by two torsional degrees of freedom that are labelled θ_1 and θ_2. θ_1 is the torsional angle between the phenyl group and the central pyridine fragment; θ_2 is the torsional angle between the two pyridine units.

Fig. S36 shows that the three knots populate the two degrees of freedom differently. As the knot becomes less tight, the central area of the plots becomes more crowded, which implies that the phenyl-bipyridine group of **3** is on average more planar than **1** and **2**.

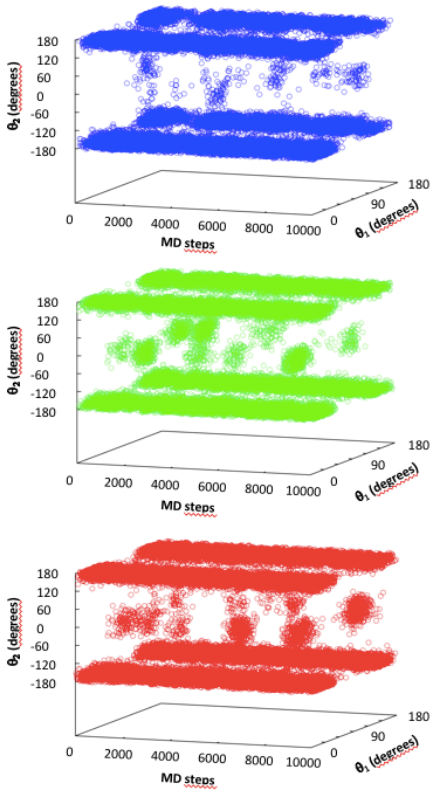

Fig. S36. Molecular Dynamics population of θ_1 (i.e. the torsional angle between the phenyl group and the central pyridine fragment) and θ_2 (i.e. the torsional angle between the two pyridine units). **1** (*top*), **2** (*centre*) and **3** (*bottom*).

The electronic spectrum of the phenyl-bipyridine moiety is highly sensitive to the values of θ_1 and θ_2, with respect to both the excitation energy and the intensity. The combination of the data of Fig. S36 and Fig. 4d of the main text allows to calculate the spectra of the three knots, see Fig. S37. It is apparent that as the knots become less tight, there is a shift to higher wavelengths of the spectral intensity. Such shift is due to the variation of θ_1 and θ_2 during the dynamics and is an intrinsic property of each knot.

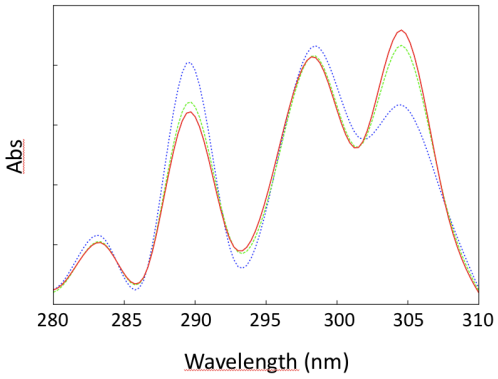

Fig. S37. Calculated spectra of **1** (blue), **2** (green) and **3** (red) obtained from the data of Fig. S36 and 4d.

The red shift is not linked to a specific conformation, but to the increase of flexibility that allows the population of more conjugated "flat conformations".

S8.4 Fragmentation pattern

The working assumption was to calculate the bond orders of the doubly charged **1** and **3**. The bond order relates to the bond strength. In a quasi-equilibrium process, the first bonds that break are those that are the weakest. We label "bond type 1" the C-O bond between the oxygen atom that is lost in **1** and the phenyl-bipyridine fragment; "bond type 2" is the C-O bond between the same oxygen atom and the bipyridine fragment. The calculations were carried out on the global minimum energy structures. In the numbering, the units follow the sequence along the knot structure. When the two types of bond have the same number, they refer to the same oxygen atom.

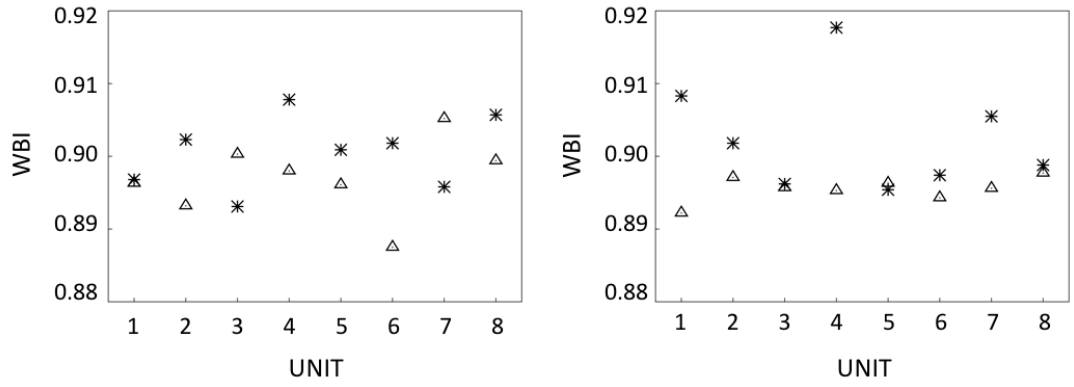

Fig. S38. Calculated bond index (WBI) for bonds of type 1 (stars) and type 2 (triangles) for doubly charged knots: **1** (left) and **3** (right).

Fig. S38 shows the calculated bond order for **1** and **3**. Some differences emerge between **1** and **3**. In knot **1**, the type 2 bond of unit 6 is weaker than the others. This is the bond that breaks initially. Additional breaking of a CO bond takes place with a much smaller

probability for the type 2 bond of unit 2 and the type 1 bond of unit 3. Because of the low probability of other processes, the dangling oxygen atom has time to re-organize its electronic structure and produce loss of a water molecule. In knot **3**, there is still a bond of type 2 that is weaker than the others, namely the type 2 bond of unit 1. However, there are several bonds of types 1 and 2 that are of comparable strength. The breaking of a CO bond is less likely or, in other words, it requires higher energy. When this CO bond breaks, other CO bonds break in a similar time scale. The dangling oxygen atom does not have time to re-organize its electronic structure and fragmentation of the knot occurs. Since the two charges of the di-cation electrostatically repel each other, thermodynamics requires that they be as far apart as possible. In practice, this can be accomplished by breaking the type 1 bond of unit 5, which is also the weakest of the type 1 bonds. The two bond cleavages produce two half knots.

References

1. Danon JJ, Krüger A, Leigh DA, Lemonnier J-F, Stephens AJ, Vitorica-Yrezabal IJ, Woltering SL (2017) *Science* 335:159–162.
2. Case DA, Darden TA, Cheatham TEIII, Simmerling CL, Wang J, Duke RE, Luo R, Walker RC, Zhang W, Merz KM, Roberts B, Wang B, Hayik S, Roitberg A, Seabra G, Kolossváry I, Wong KF, Paesani F, Vanicek J, Liu J, Wu X, Brozell SR, Steinbrecher T, Gohlke H, Cai Q, Ye X, Wang J, Hsieh M-J, Cui G, Roe DR, Mathews DH, Seetin MG, Sagui C, Babin V, Luchko T, Gusarov S, Kovalenko A, Kollman PA (2010) AMBER 12 (University of California, San Francisco).
3. Wang J, Wolf RM, Caldwell JW, Kollman PA, Case DAJ (2004) *Comput Chem* 25:1157−1174.
4. Wang J, Wang W, Kollman PA, Case DAJ (2006) *Mol Graph Model* 25:247260.
5. Darden T, York D, Pedersen LJ (1993) *Chem Phys* 98:10089−10092.
6. Ryckaert J-P, Ciccotti G, Berendsen HJCJ (1977) *Comput Phys* 23:327−341.
7. Humphrey W, Dalke A, Schulten KJ (1996) *Mol Graph* 14:33−38.
8. Daidone I, Amadei A (2012) *WIREs Comput Mol Sci* 2:762−770.
9. Spectus CON (2008) *Density Functionals with Broad Applicability in Chemistry.* 41:157–167.
10. Frisch MJ, Trucks GW, Schlegel HB, Scuseria GE, Robb MA, Cheeseman JR, Scalmani G, Barone V, Mennucci B, Petersson GA et al. (2009) Gaussian 09 (Gaussian, Inc., Wallingford CT).
11. Barone V, Cossi M (1998) *J Phys Chem A* 102:1995-2001; Cossi M, Rega N, Scalmani G, Barone V (2003) *J Comp Chem* 24:669–81.